

Efficient and High Fidelity Incorporation of dCTP Opposite 7,8-Dihydro-8-oxodeoxyguanosine by *Sulfolobus solfataricus* DNA Polymerase Dpo4*[§]

Received for publication, October 5, 2005, and in revised form, November 16, 2005. Published, JBC Papers in Press, November 22, 2005, DOI 10.1074/jbc.M510889200

Hong Zang, Adriana Irimia, Jeong-Yun Choi, Karen C. Angel, Lioudmila V. Loukachevitch, Martin Egli, and F. Peter Guengerich¹

From the Department of Biochemistry and Center in Molecular Toxicology, Vanderbilt University School of Medicine, Nashville, Tennessee 37232-0146

DNA polymerases insert dATP opposite the oxidative damage product 7,8-dihydro-8-oxodeoxyguanosine (8-oxoG) instead of dCTP, to the extent of >90% with some polymerases. Steady-state kinetics with the Y-family *Sulfolobus solfataricus* DNA polymerase IV (Dpo4) showed 90-fold higher incorporation efficiency of dCTP > dATP opposite 8-oxoG and 4-fold higher efficiency of extension beyond an 8-oxoG:C pair than an 8-oxoG:A pair. The catalytic efficiency for these events (with dCTP or C) was similar for G and 8-oxoG templates. Mass spectral analysis of extended DNA primers showed $\geq 95\%$ incorporation of dCTP > dATP opposite 8-oxoG. Pre-steady-state kinetics showed faster rates of dCTP incorporation opposite 8-oxoG than G. The measured $K_{a,dCTP}$ was 15-fold lower for an oligonucleotide containing 8-oxoG than with G. Extension beyond an 8-oxoG:C pair was similar to G:C and faster than for an 8-oxoG:A pair, in contrast to other polymerases. The E_a for dCTP insertion opposite 8-oxoG was lower than for opposite G. Crystal structures of Dpo4 complexes with oligonucleotides were solved with C, A, and G nucleoside triphosphates placed opposite 8-oxoG. With ddCTP, dCTP, and dATP the phosphodiester bonds were formed even in the presence of Ca^{2+} . The 8-oxoG:C pair showed classic Watson-Crick geometry; the 8-oxoG:A pair was in the *syn:anti* configuration, with the A hybridized in a Hoogsteen pair with 8-oxoG. With dGTP placed opposite 8-oxoG, pairing was not to the 8-oxoG but to the 5' C (and in classic Watson-Crick geometry), consistent with the low frequency of this frameshift event observed in the catalytic assays.

Reactive chemicals can cause damage to DNA, regardless of whether the source is exogenous (e.g. chemicals in the environment) or endogenous origin (e.g. reactive oxygen species or lipid peroxidation products) (1–3). The damage to DNA, if not repaired, can result in blockage of replication

* This work was supported in part by United States Public Health Service Grants R01 ES010375 and P30 ES000267. The use of the advanced Photon Source was supported by the United States Department of Energy, Basic Energy Sciences, Office of Science under contract W-31-109-Eng-38. The DuPont-Northwestern-Dow Collaborative Access Team Synchrotron Research Center at the Advanced Photon Source (Sector 5) was supported by E. I. DuPont de Nemours & Co., the Dow Chemical Co., the National Science Foundation, and the State of Illinois. The costs of publication of this article were defrayed in part by the payment of page charges. This article must therefore be hereby marked "advertisement" in accordance with 18 U.S.C. Section 1734 solely to indicate this fact.

The atomic coordinates and structure factors (codes 2C22, 2C2D, 2C2E, 2C28 and 2C2R) have been deposited in the Protein Data Bank, Research Collaboratory for Structural Bioinformatics, Rutgers University, New Brunswick, NJ (<http://www.rcsb.org/>).

[§] The on-line version of this article (available at <http://www.jbc.org/>) contains Figs. S1–S2 and Tables S1–S3.

¹ To whom correspondence should be addressed: 638 Robinson Research Bldg., 23rd and Pierce Aves., Nashville, TN 37232-0146. Tel.: 615-322-2261; Fax: 615-322-3141; E-mail: f.guengerich@vanderbilt.edu.

and transcription or, if the damage is bypassed, the introduction of errors into the genome (3, 4). DNA modifications can cause mutations in all species, and several lines of evidence exist to support the proposal that cancer and other diseases can be caused by DNA damage (5, 6).

8-OxoG² is a major lesion arising from oxidative stress in lower organisms and eukaryotes, although the actual reported levels vary considerably because of artifacts in measurement (7, 8). This lesion is of interest not only in consideration of cancer (9, 10) but has also been associated with aging (11), infertility (12), and hepatitis (13). Although 8-oxoG can be oxidized further to *spiro* products that are even more mutagenic in some assay systems (14, 15), the relevance of those products is unclear in that they remain to be identified *in vivo*, with the exception of base excision repair-deficient *Escherichia coli* exposed to high concentrations of chromate (16).

The molecular basis of miscoding by 8-oxoG has been the subject of investigation since the discovery of this lesion in DNA. Originally the lesion was reported as 8-hydroxyguanine; NMR studies (17) defined the structure as the tautomer 8-oxoG, with chemistry of the N-7 atom changed from that of a nucleophile to an amide nitrogen. In all biological systems examined, a proclivity for binding to or insertion of A is observed. The T_m for the 8-oxoG:A pair is $\sim 6^\circ C$ lower than a normal T:A pair, but the T_m for the 8-oxoG:C pair in the same context is $35^\circ C$ lower than for a G:C base pair (18). Thus one might expect pairing of an A with 8-oxoG to be favored over that of a C (with 8-oxoG) from thermodynamic considerations. NMR and x-ray diffraction studies of 8-oxoG pairing in oligonucleotides have been reported, and the similarity of an 8-oxoG:A pair to a T:A pair has been noted (18–20). Another feature of the binding of 8-oxoG to A in double-stranded oligonucleotides is the *anti* to *syn* shift of the 8-oxoG glycosidic bond, yielding a flip of the base to change the position of the atoms and facilitate pairing to A.

Although the insertion of A opposite 8-oxoG is the most common outcome (and subsequently yields a G to T transition), the biological response varies considerably (21). In early work in the field, Shibutani *et al.* (22) noted considerable variation among polymerases in their tendencies to insert dATP *versus* dCTP. Although the parameters used in the literature vary, the extent of misincorporation ranges from about 5 to 95% among different DNA polymerases (22–30). On the basis of steady-state kinetic parameters, *E. coli* polymerases I and II (exo⁻), bacteriophage pol T7, rat pol β , and bovine pol δ insert dATP opposite 8-oxoG in 30–50% of the events (23–25, 28, 29, 31), and DNA polymerase pol α (22), human immunodeficiency virus type 1 reverse tran-

² The abbreviations used are: 8-oxoG, 7,8-dihydro-8-oxodeoxyguanosine; CID, collision-induced dissociation; Dpo4, *Sulfolobus solfataricus* S2 DNA polymerase IV; DTT, dithiothreitol; E_a , activation energy; HPLC, high performance liquid chromatography; MS, mass spectrometry; pol, polymerase; r.m.s., root mean square; LC, liquid chromatography.

(1)	5' -GGGGAAGGATTC-	3'
(2)	3' -CCCCTCCTAAGXCACT-	5'
(3)	5' -GGGGAAGGATTC-	3'
(2)	3' -CCCCTCCTAAGXCACT-	5'
(4)	5' -GGGGAAGGATTC-	3'
(2)	3' -CCCCTCCTAAGXCACT-	5'
(5)	5' -GGGGAAGGAUTC-	3'
(2)	3' -CCCCTCCTAAGXCACT-	5'
(6)	5' -GCCTCGAGCCAGCCGAGCGCUG-	3'
(7)	3' -CGGAGCTCGGTCGGCGTCTGCGACXCTCCTG-	5'

SCHEME 1. Oligonucleotide sequences used in this work.

scriptase (24), and *Bacillus stearothermophilus* pol BF (27) are particularly prone to insert dATP > dCTP. Of the DNA polymerases reported, only RB69 (26) and *Saccharomyces cerevisiae* pol η (30, 32) insert dCTP in ~95% of the incorporation events instead of dATP. Furthermore, the patterns of incorporation of 8-oxo-dGTP opposite template C versus A do not match the patterns of incorporation of dCTP versus dATP opposite 8-oxoG, indicating the asymmetry of the system (25).

Another issue is the variable tendency of DNA polymerases to extend beyond 8-oxoG:C lesions. To date reports on individual DNA polymerases indicate a general tendency to extend primers more efficiently beyond the 8-oxoG:A than the 8-oxoG:C pairs (22–24, 26, 33, 34), except for the one case of yeast pol η (32). Four x-ray structures of DNA polymerases bound to oligonucleotides containing 8-oxoG have been reported to date (26–29), and some details of these vary, e.g. the localized inversion of the dCTP phosphate in pol β (28).

Most of the work with 8-oxoG done to date has been with replicative DNA polymerases and relatively little has been done with the more recently discovered translesion polymerases, except for the yeast pol η studies already mentioned (30, 32). A recent Carlson and Washington (30) article with *S. cerevisiae* pol η is of note in that pre-steady-state kinetics indicated that the efficiency (k_{pol}/K_d) for dCTP opposite 8-oxoG was still ~50% that of the opposite G, which is unusual compared with our own work with replicative polymerases (23, 24, 31). Archebacter DNA polymerase Dpo4 is a model for translesion synthesis (for a recent discussion of mechanisms, see Ref. 35). We analyzed the interaction of Dpo4 with 8-oxoG using MS, steady-state and pre-steady-state kinetics, and x-ray crystallography. Although the translesion DNA polymerases are often assumed to be rather error prone, we find that Dpo4 shows high fidelity in inserting dCTP opposite 8-oxoG and that this pair is very efficiently extended. Consistent with the activity data, the crystal structures of ternary complexes of Dpo4 with dCTP and ddCTP opposite 8-oxoG reveal standard Watson-Crick geometry of the pairs. Conversely, dATP forms a Hoogsteen pair with 8-oxoG, with the latter adopting *syn* geometry. All three complexes belong to the "Type I" crystal form described for the ternary complexes with native DNA (36). Thus, 8-oxoG constitutes the single template base present at the active site. However, in both complexes with dCTP and ddCTP the primer was extended by a single C and, in the complex with dATP, the structural data indicate the presence of a second nucleoside triphosphate immediately adjacent to the active site. The complexes with dGTP and ddGTP belong to the "Type II" form (36), with two template bases present at the active site, whereby 8-oxoG is skipped and the nucleoside triphosphates engage in a Watson-Crick base pair with the C 5'-adjacent to the modified base. This arrangement is similar to that found in the ternary complex of dGTP with a template-primer construct containing 1,*N*²-ethenodeoxyguanosine (37) and helps to rationalize the low frequency frameshift with G opposite 8-oxoG in the *in vitro* primer extension studies.

EXPERIMENTAL PROCEDURES

Reagents—Dpo4 was expressed in *E. coli* and purified using heat denaturation, Ni²⁺-nitriloacetate chromatography, and ion-exchange chromatography as described elsewhere (37). All oligonucleotides used in this work were synthesized by Midland Certified Reagent Co. (Midland, TX) and purified using HPLC by the manufacturer, with analysis by matrix-assisted laser desorption-time of flight MS.

Polymerization Assays and Gel Electrophoresis—A ³²P-labeled primer, annealed to either an unmodified or adducted template, was extended in the presence of the individual dNTPs (Scheme 1). In the preliminary "run-on" assays, each reaction was initiated by adding 2 μ l of dNTP-Mg²⁺ solution (final concentrations of 250 μ M of each dNTP and 5 mM MgCl₂) to a preincubated E·DNA complex (final concentrations of 50 mM Tris-HCl (pH 7.8), 100 nM DNA duplex, 100 nM Dpo4, 5 mM DTT, 50 μ g of bovine serum albumin ml⁻¹, 50 mM NaCl, and 5% glycerol (v/v)) at 37 °C, yielding a total reaction volume of 8 μ l. After varying lengths of time, reactions were quenched with 50 μ l of 20 mM EDTA (pH 9.0) in 95% formamide (v/v).

Aliquots (3 μ l) were separated by electrophoresis using denaturing gels containing 8.0 M urea and 16% acrylamide (w/v) (from a 19:1 acrylamide:bisacrylamide solution (w/w), AccuGel, National Diagnostics, Atlanta, GA) with 80 mM Tris borate buffer (pH 7.8) containing 1 mM EDTA. The gel was exposed to a phosphorimager screen (Imaging Screen K, Bio-Rad) overnight. The bands (representing extension of the primer) were visualized with a phosphorimaging system (Bio-Rad, Molecular Imager® FX) using the manufacturer's Quantity One Software, version 4.3.0.

Steady-state Kinetics—Unless indicated otherwise, all Dpo4 reactions were performed at 37 °C in 50 mM Tris-HCl buffer (pH 7.8) containing 5% glycerol (v/v), 5 mM DTT, 50 mM NaCl, and 50 μ g of bovine serum albumin ml⁻¹. For both unmodified and modified templates, the molar ratio of the primer-template to enzyme was 10:1 to 40:1, and the reactions were done at eight dNTP concentrations (reaction time of 20 s to 3 min).

LC-MS Analysis of Oligonucleotide Products from Dpo4 Reactions—Dpo4 reactions were performed at 37 °C for 4 h in 50 mM Tris-HCl buffer (pH 7.8) containing 5% glycerol (v/v), 5 mM DTT, 50 mM NaCl, 5 mM MgCl₂, and 100 μ g of bovine serum albumin ml⁻¹. The reactions were done with 10 μ M oligonucleotide substrate, 5 μ M Dpo4, and four dNTPs at 1 mM each, in a final reaction volume of 100 μ l. The reaction was terminated by extraction of excess dNTPs using a spin column (Bio-Spin 6 chromatography column, Bio-Rad). To the above filtrate (120 μ l), concentrated Tris-HCl, DTT, and EDTA were added to restore the initial concentrations, and uracil DNA glycosylase solution was added (20 units) (37). The reaction was incubated at 37 °C for 6 h to hydrolyze the uracil residue on the extended primer. The final reaction mixture was then heated at 95 °C for 1 h in the presence of 0.25 M piperidine, followed by removal of

TABLE 1

Crystal data and refinement parameters for the ternary Dpo4-DNA-dNTP (ddNTP) complexes

Parameter	Dpo4-dG	Dpo4-dA	Dpo4-dC	Dpo4-ddG	Dpo4-ddC
X-ray source	APS, SER-CAT	ALS	APS, IMCA-CAT	APS, DND-CAT	APS, IMCA-CAT
Beamline	BM-22	8.2.1.	ID-17	ID-5	ID-17
Detector	MARCCD	Quantum CCD	Quantum CCD	MARCCD	Quantum CCD
Wavelength (Å)	0.98	1.00	1.00	1.00	1.00
Temperature (K)	110	110	110	110	110
No. of crystals	1	1	1	1	1
Space group	<i>P</i> 2 ₁ 2 ₁ 2				
Unit cell (<i>a</i> , <i>b</i> , <i>c</i> ; Å)	93.27,103.91,52.49	97.50,102.01,53.10	96.03,100.39,52.41	93.35,102.03,52.83	95.20,100.15,52.00
Resolution range (Å)	32.47–2.56	43.99–2.56	44.49–2.60	31.96–2.27	42.99–2.55
Highest resolution shell ^a	(2.72–2.56)	(2.72–2.56)	(2.76–2.60)	(2.42–2.27)	(2.71–2.55)
No. of measurements	116,072	166,580	55,584	168,882	60,782
No. of unique reflections	17,101	17,022	14,985	23,827	16,653
Redundancy	6.78	9.78	3.7	7.8	3.64
Completeness (%)	99.8 (100)	97.0 (81.7)	93.1 (89.4)	99.7 (100)	98.8 (93.9)
<i>R</i> -merge ^b (%)	7.4	9.4	12.0	6.2	12.5
Signal to noise (<342I/σI)	7.9	16.5	10.7	10.4	8.8
Solvent content (%)	51.9	54.3	52.5	51.0	51.1
Model composition (asymmetric unit)					
No. of amino acid residues	341	341	341	341	341
No. of water molecules	111	96	112	98	106
No. of Ca ²⁺ ions	3	5	3	3	4
No. template nucleotides	17	15	15	17	16
No. of primer nucleotides	13	13	14	13	14
No. of dGTP	1				
No. of dATP		2			
No. of dCTP			1		
No. of ddGTP				1	
No. of ddCTP					1
<i>R</i> _f ^c (%)	23.0	24.0	26.7	23.9	25.1
<i>R</i> -free ^d (%)	26.4	28.0	31.5	25.6	31.0
Estimated coordinate error (Å)					
From Luzatti plot	0.36	0.43	0.45	0.35	0.41
From Luzatti plot (c-v) ^e	0.42	0.53	0.55	0.4	0.53
From σA plot	0.34	0.54	0.69	0.34	0.49
From σA plot (c-v) ^e	0.38	0.63	0.77	0.41	0.5
Temperature factors					
From Wilson plot (Å ²)	57.9	80.9	44.2	56.2	55.1
mean isotropic (Å ²)	51.6	78.6	57.2	53.8	54.6
r.m.s. deviation in temperature factors					
Bonded main chain atoms (Å ²)	1.3	1.6	1.4	1.5	1.3
Bonded side chain atoms (Å ²)	2.0	1.7	1.7	2.2	1.7
r.m.s. standard deviation from ideal values					
Bond lengths (Å)	0.008	0.011	0.008	0.008	0.009
Bond angles (°)	1.3	1.9	1.6	1.4	1.4
Dihedral angles (°)	22.8	22.2	22.6	22.32	22.3
Improper angles (°)	1.0	1.2	1.3	1.1	1.4

^a Values in parentheses correspond to the highest resolution shells.^b *R*-merge = $\sum_{h,k,l} \sum_{j=1, \dots, N} |I_{h,k,l} - \langle I_{h,k,l} \rangle| / \sum_{h,k,l} \sum_{j=1, \dots, N} I_{h,k,l}$, where the outer sum (*h*, *k*, *l*) is taken over the unique reflections.^c *R*_f = $\sum_{h,k,l} \|F_{oh,k,l} - k|F_{ch,k,l}| / \sum_{h,k,l} |F_{oh,k,l}|$, where $|F_{oh,k,l}|$ and $|F_{ch,k,l}|$ are the observed and calculated structure factor amplitudes, respectively.^d *R*-free idem, for the set of reflections (5% of the total) omitted from the refinement process.^e c-v, cross-validation.

solvent by lyophilization. The dried residues were dissolved in 100 μl of H₂O for the following MS analysis.

MS was performed on a DecaXP ion trap instrument (ThermoFinnigan, San Jose, CA). Separation of oligonucleotides was carried out with a Jupiter microbore column (1.0 × 150 mm, 5 μm, Phenomenex, Torrance, CA). Buffer A contained 10 mM NH₄CH₃CO₂ (pH 6.8) and 2% CH₃CN (v/v); buffer B contained 10 mM NH₄CH₃CO₂ (pH 6.8) and 95% CH₃CN (v/v). The following gradient program was used with a flow rate of 1.0 ml min⁻¹: 0–2 min, hold at 100% A; 2–20 min, linear program to 100% B; 20–30 min, hold at 100% B; 30–31 min, linear program to 100% A; 31–40 min, hold at 100% A (for next injection). The desired oligonucleotide products were eluted at ~8 min. A pre-column “Tee” set-up

was applied, with only 10% of the total flow infused to the ion source. The fast flow rate helped reduce the equilibration time of the column, and thus the retention time of the oligonucleotides was consistent between runs. Samples were infused using an autosampler, with 8 μl withdrawn from a 50-μl reaction. Electrospray conditions were: source voltage, 3.4 kV; source current, 8.5 μA; sheath gas flow rate setting, 28.2; auxiliary sweep gas flow rate setting, 4.3; capillary voltage, -49 V; capillary temperature, 230 °C; and tube lens voltage, -67 V. MS/MS conditions were: normalized collision energy, 35%; activation Q, 0.250; time, 30 ms; 1 scan. Product ion spectra were acquired over the *m/z* 250–2000 range. The abundant ions from LC-MS spectra were selected for CID analysis, and the cut-off was set above ~15% of the most abun-

dant ion. When more than one ion came from a single species, the peak responding to the doubly charged parent ion was chosen for fragmentation analysis. The calculations of the CID fragmentations of a certain oligonucleotide sequence were done using a program linked to the Mass Spectrometry Group of Medicinal Chemistry at the University of Utah.

Pre-steady-state Kinetics—Pre-steady-state kinetics were performed using a KinTek model RQF-3 chemical quench flow apparatus (KinTek Corp., Austin, TX) with 50 mM Tris-HCl (pH 7.8) buffer in the drive syringes. The reactions were initiated by mixing the pre-equilibrated polymerase-DNA complex (containing 100 mM Tris-HCl, pH 7.8, 200 nM ^{32}P -labeled DNA duplex, 5 mM DTT, 100 μg of bovine serum albumin ml^{-1} , 50, 200, or 300 nM Dpo4, 50 mM NaCl, and 5% glycerol (v/v)) in sample syringe A (12.5 μl) with either dNTP-Mg $^{2+}$ (40–400 μM dNTP, depending on the oligonucleotide sequence) or 10 mM MgCl $_2$ from syringe B (10.9 μl) at 37 °C. The reactions were quenched with 0.6 M EDTA (pH 9.0) in syringe C after reaction times that varied from 0.1 to 30 s. Reactions were combined with 500 μl of formamide dye solution (20 mM EDTA, 95% formamide (v/v), and 0.05% bromophenol blue (w/v)), and the components were separated by electrophoresis (3 μl of the sample) on a denaturing gel, with analysis as described for gel electrophoresis of polymerization reactions. The resulting plot (of product con-

centration *versus* time) was fit to the burst equation, $y = A(1 - e^{-k_p t}) + k_{ss}t$, where A represents burst amplitude, k_p is the pre-steady-state rate of nucleotide incorporation, t is time, and k_{ss} is the steady-state rate of nucleotide incorporation, and analyzed using GraphPad Prism version 3.0a (San

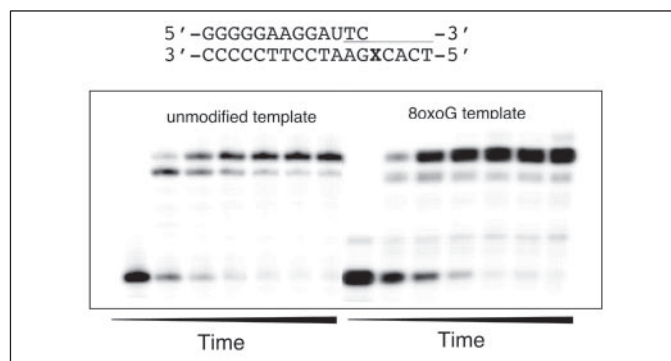
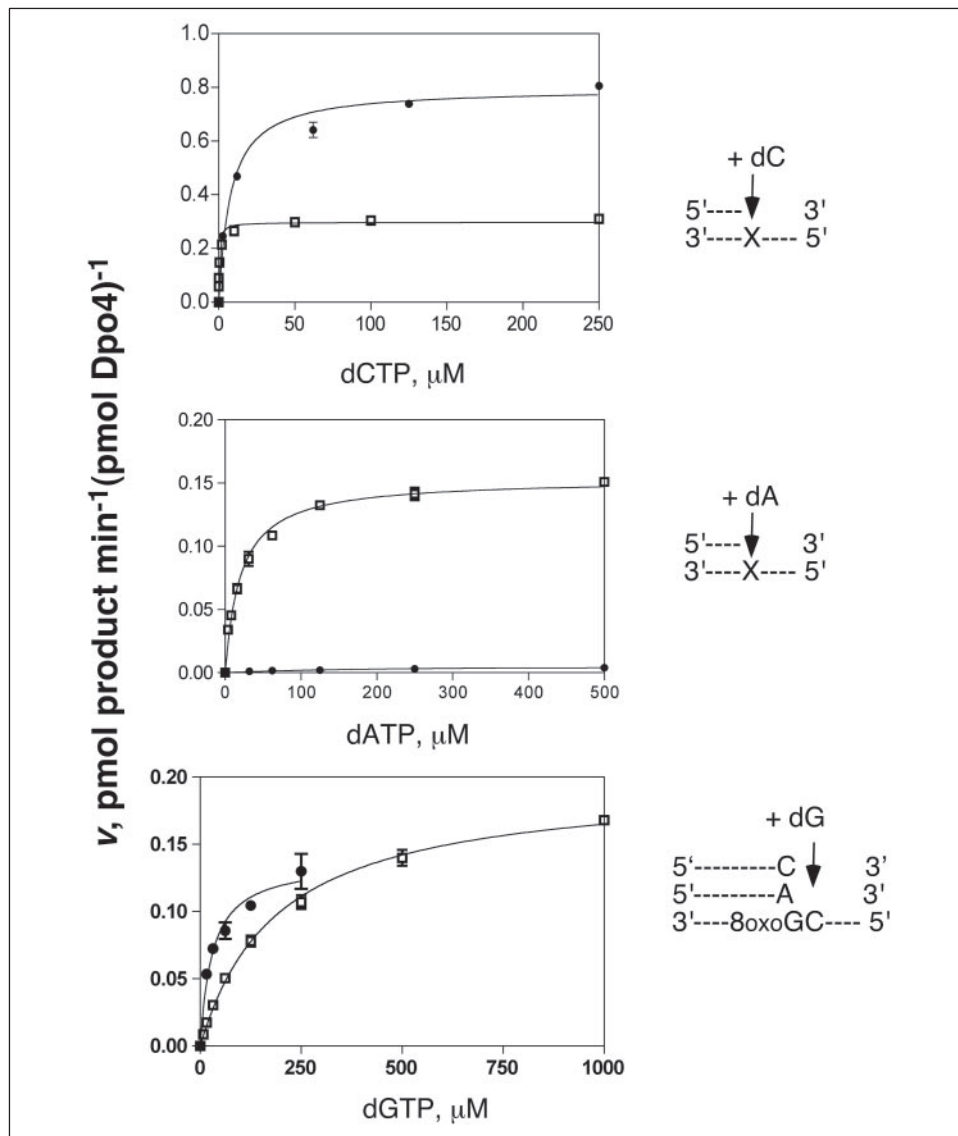


FIGURE 1. **Extension of primers by Dpo4.** Extension of a ^{32}P -labeled primer (13-mer, oligomer 1 of Scheme 1) opposite G or 8-oxoG (oligomer 2 of Scheme 1) was analyzed with increasing reaction times, as indicated by the gradient bars (0, 10, 30, 60, 90, 120, and 180 min, respectively).

FIGURE 2. **Steady-state kinetic analysis of incorporation and extension of primers by Dpo4.** *Top*, incorporation of dCTP into the primer (oligomer 1, Scheme 1) opposite G (●) or 8-oxoG (□) in the template (oligomer 2 of Scheme 1). The dCTP concentration was varied from 1 to 500 μM for incorporation opposite G and from 0.05 to 500 μM for incorporation opposite 8-oxoG. *Center*, incorporation of dATP into the primer (oligomer 1, Scheme 1) opposite G (●) or 8-oxoG (□) in the template (oligomer 2 of Scheme 1). *Bottom*, incorporation of dGTP in a primer with either C (●) or A (□) (primer 3 or 4, respectively, Scheme 1) opposite 8-oxoG of the template (oligomer 2, Scheme 1). See Table 2 for calculated parameters.



dNTP Incorporation Opposite 8-OxoG by Pol Dpo4

Diego, CA). In subsequent analyses with multiple dNTP concentrations, the results were fit to the hyperbolic expression $k_p = (k_{\text{pol}}[\text{dNTP}]) / ([\text{dNTP}] + K_d, \text{dNTP})$, using GraphPad Prism.

Crystallization of Dpo4-DNA Complexes—For the crystallizations of ternary complexes with either ddNTPs or dNTPs we used the 18-mer template 5'-TCAC(8-oxoG)GAATCCTTCCCC-3' (2, Scheme 1) and the 13-mer primer 5'-GGGGGAAGGATTC-3' (1, Scheme 1). All Dpo4 crystallizations were performed as described (37), with the exception that the concentrations of the nucleoside triphosphates were either 1 or 5 mM, and the concentrations of d(dNTP) in the cryoprotectant solutions were 5 mM. Only Ca^{2+} was added to the annealing and reservoir solutions and EDTA was used to mask traces of Mg^{2+} in all experiments. Crystals were also grown of a binary complex between the 18-mer template (2, Scheme 1) and the 14-mer primer 5'-GGGGGAAGGATTC-3' (3, Scheme 1) with C opposite 8-oxoG. Although these crystals diffracted to high resolution, they showed persistent twinning and we subsequently did not pursue structure determination of that particular product complex.

X-ray Diffraction Data Collection and Processing—Diffraction data sets for Dpo4 ternary complex crystals were collected at 110 K using a synchrotron radiation wavelength of 1.0 Å on beamlines at the Advanced Photon Source (APS), Argonne, IL (SER-CAT BM-22, Dpo4-dGTP = Dpo4-dG; IMCA-CAT ID-17, Dpo4-dCTP = Dpo4-dC and Dpo4-ddCTP = Dpo4-ddC; DND-CAT ID-5, Dpo4-ddGTP = Dpo4-ddG), or at the Advanced Light Source (ALS), Berkeley, CA (8.2.1, Dpo4-dATP = Dpo4-dA) (Table 1). The high resolution limit of diffraction for these crystals lies within a range of 2.27 to 2.6 Å. Data to 3.13-Å resolution were also collected for the Dpo4-ddA complex but this structure was not refined. Indexing and scaling with the Dpo4-dG and Dpo4-ddG complexes were performed using the program X-GEN (38); for the Dpo4-dA, Dpo4-dC, and Dpo4-ddC complexes the program XDS (39) was used. Autoindexing and systematic absences indicated the space group $P2_12_12$ for all structures. The data were further processed using CCP4 package programs, including the truncate procedure performed with TRUNCATE (40). The resulting data sets for the Dpo4-dG and Dpo4-ddG complexes are of very good quality as indicated by *R*-merge values of 7.4 and 6.2%, respectively. The Dpo4-dA, Dpo4-dC, and Dpo4-ddC data sets show slightly inferior quality because of high mosaicity, the *R*-merge values are 9.4, 12.0, and 12.5%, respectively (see Table 1 for statistics of data processing and data quality). It should also be noted that the crystals formed by the Dpo4-dA, -dC, and -ddC ternary complexes in general had a higher tendency to be twinned.

Structure Determination and Refinement—Because of the similar values of the unit cell constants of the Dpo4-dG and Dpo4-ddG crystal structures (this work) and the ternary complex of Dpo4 with 1, N^2 -ethenoG-modified DNA and ddGTP (Dpo4-4 complex; Protein Data Bank code 2br0 (37)), the refined model of the latter structure (minus solvent molecules) was used as a starting model for the Dpo4-dG and Dpo4-ddG structures. The initial positions of the models were optimized by several rounds of rigid body refinement, gradually increasing the resolution of the diffraction data.

The Dpo4-dA, Dpo4-dC, and Dpo4-ddC structures were solved by molecular replacement with the program Phaser (41), using the refined 2.27-Å resolution structure of the Dpo4-ddG complex, devoid of all side chains and solvent molecules, as the search model. The positioned models gave values for Rotation Function Z of 27.3 (for Dpo4-dA), 27.2 (for Dpo4-dC), and 24.8 (for Dpo4-ddC). The values for the Translation Function Z were 17.9, 16.0, and 14.3, respectively, at 3.5-Å resolution. The locations of the models containing the side chains were optimized

by several rounds of rigid body refinement. Data of increasing resolution were included in the refinement until the diffraction limit was reached.

The TURBO-FRODO program (version OpenGL.1) was used for manual model rebuilding into σA maps computed using modified σA coefficients (42). The initial difference Fourier maps showed clear negative density (higher than 5.0 r.m.s. deviation) for Ca^{2+} ions as well as for the (d)dNTP used in the crystallizations. Unambiguous density was also observed for the DNA duplex except for the first three template nucleotides (5'-TCA) that were partly or fully disordered in all structures. Therefore, in the absence of density, the 5'-terminal nucleotides of the template were completely omitted from the models in some of the structures (see Table 1 for model composition in each case). Clear density was seen in the initial difference Fourier electron density maps for a 14th nucleotide added by the polymerase to the 13-mer primer in the Dpo4-dC and Dpo4-ddC structures.

Refinements were performed using the program CNS (43). Five percent of the reflections were excluded from the refinement to calculate the cross-validation residual *R*-free. Water oxygen atoms were added into positive regions (higher than 3.0 standard deviation) of ($F_o - F_c$) Fourier difference electron density during the manual model rebuilding steps. Current statistics of the refined models for all structures are presented in Table 1.

The standard procedures in CNS (43) and PROCHECK (44) were used to inspect the quality and stereochemistry of the five models. The crystallographic figures were prepared using Pymol. Atomic coordinates and measured structure factor amplitudes for the Dpo4-dG, -dA, -dC, -ddG, and -ddC complexes have been deposited in the Protein Data Bank with accession codes 2c22, 2c2d, 2c2e, 2c28, and 2c2r, respectively.

RESULTS

General Strategy—Dpo4 has several features that provide advantages as a model polymerase, including the availability of several crystal structures with modified DNA (37, 45–47) and detailed kinetic analysis (48, 49). Preliminary analysis of dNTP incorporation opposite 8-oxoG by Dpo4 suggested that this was a low error process, *i.e.* dCTP was inserted most frequently. The variability in ratios of insertion of dATP *versus* dCTP opposite 8-oxoG by different polymerases has been known to be considerable (22), and the interaction of Dpo4 with a DNA template containing 8-oxoG was used as a model for understanding miscoding on a structural and kinetic basis.

Full-length Extension of Oligonucleotide Primers by Dpo4 in the Presence of All Four dNTPs—Initial experiments with Dpo4 were done with a primer-template complex based on earlier studies (37), with a uracil residue placed in the primer strand in place of T to facilitate subsequent MS analysis (see below) (Fig. 1). In these qualitative experiments done with a single high concentration of the dNTP mixture, extension of the primer to full-length product was similar with templates containing either 8-oxoG or G in the same position (Fig. 1).

Steady-state Kinetic Analysis of dNTP Insertion and Extension by Dpo4—Preliminary analysis indicated that Dpo4 inserted dNTPs opposite 8-oxoG in the order $C > A > G > T$ (results not shown). The system was analyzed in more detail using steady-state kinetics (Fig. 2, Table 2). When insertion was opposite an unmodified G, insertion of dATP or dGTP was $>10^3$ less efficient than dCTP (Table 2). For insertion opposite 8-oxoG, the order was dCTP $>$ dATP $>$ dGTP, with an order of magnitude or more difference in catalytic efficiency (k_{cat}/K_m) in each pair of comparisons. The insertion of dCTP opposite G and 8-oxoG showed similar catalytic efficiency, even with differences in the trends for k_{cat} and K_m (Table 2).

TABLE 2
Steady-state kinetic parameters for 1-base incorporation reaction by Dpo4

Oligomer pair (Scheme 1)	Primer-template pair	dNTP	k_{cat} min^{-1}	K_m μM	k_{cat}/K_m $\text{min}^{-1} \mu\text{M}^{-1}$
1	-↓	dCTP	0.80 ± 0.02	7.7 ± 1.1	0.10 ± 0.02
2	-G-				
1	-↓	dCTP	0.30 ± 0.01	0.44 ± 0.10	0.68 ± 0.10
2	-8-oxoG-				
1	-↓	dATP	0.005 ± 0.001	180 ± 24	0.00003 ± 0.00001
2	-G-				
1	-↓	dATP	0.15 ± 0.003	20 ± 1	0.0075 ± 0.0004
2	-8-oxo G-				
1	-↓	dGTP	0.041 ± 0.001	86 ± 13	0.0005 ± 0.0001
2	-G-				
1	-↓	dGTP	0.023 ± 0.001	28 ± 7	0.0008 ± 0.0002
2	-8-oxo G-				
3	-C-↓	dGTP	0.39 ± 0.02	66 ± 8	0.0059 ± 0.0008
2	-G-C-				
3	-C-↓	dGTP	0.14 ± 0.01	30 ± 6	0.0047 ± 0.0010
2	-8-oxoG-C-				
4	-A-↓	dGTP	0.011 ± 0.001	57 ± 14	0.0002 ± 0.0001
2	-G-C-				
4	-A-↓	dGTP	0.20 ± 0.01	190 ± 12	0.0011 ± 0.0001
2	-8-oxoG-C-				

In previous work with other polymerases, an 8-oxoG:A pair has generally been extended more efficiently than an 8-oxoG:C pair (22–26, 33, 34). In the sequence used in this work, insertion of dGTP opposite C (a normal pairing) in the position 5' used in the first part of the experiments was considerably less efficient because of a much higher K_m value (and a somewhat lower k_{cat}) (Table 2). The reason for this difference is unknown. However, extension beyond the 8-oxoG:C pair was as efficient as beyond a G:C pair in this setting. Extension beyond an 8-oxoG:A pair was ~4-fold less efficient (Table 2, Fig. 2, *bottom panel*), in contrast to most reports with DNA polymerases (22–26, 33, 34) with the exception of yeast pol η (32).

MS Analysis of Dpo4 Oligonucleotide Products—In recent work with Dpo4 (37) and other DNA polymerases, simple electrophoretic gel analyses of polymerization have been found to be deficient in the analysis of patterns of nucleotide incorporation, in that some unusual events (*e.g.* multiple dNTP additions) are observed in incubations with single dNTPs that are not common in studies with all four dNTPs present. In the approach used here, a primer is fully extended and MS is used to analyze the composition of the product (37). A uracil in the primer, several bases 5' of the first site of incorporation and paired with A, appears not to modify the polymerization process. This uracil allows the extended primer to be cut with uracil DNA glycosylase to make it smaller and facilitate MS/CID analysis in an ion-trap instrument.

The product of extension of primer 5 (Scheme 1) placed opposite template 2 (containing 8-oxoG) was analyzed as described. The products eluted from HPLC together at t_R 8.5 min (Fig. 3A), and analysis of the peak yielded ions at m/z 1087.3 and 724.6, which were -2 and -3 ions, respectively (Fig. 3B). Reconstruction of the m/z 1087.3 HPLC profile yielded the chromatogram shown in Fig. 3C, and CID analysis of the m/z 1087.3 ion produced the fragmentation pattern shown in Fig. 3D. Comparison of the major ions with those possible for several oligonucleotides (supplementary data Table 1S) indicated the sequence 5'-pTCCGTGA-3', corresponding to the insertion of C opposite the 8-oxoG in the template.

Further inspection of the initial mass spectrum shown in Fig. 3B indicated the presence of an ion at m/z 1099.0. This m/z value corresponds to an M_r of 2200.0 and a -2 charge, consistent with a product containing an A inserted opposite the 8-oxoG. CID analysis of this peak in the manner described above provided further evidence for this assignment (supplementary data Figs. 1S, A and B, and Table S2). The

expected -3 ion was not observed in this case. Reconstruction analysis (as in Fig. 3C) and comparisons indicate that the extent of dATP incorporation is ~5% that of dCTP, a result consistent with that predicted by comparison of the catalytic efficiencies in the steady-state kinetic analysis with individual dNTPs (Table 2).

The insertion analysis was also done with a longer oligonucleotide to establish if the proclivity to insert dCTP opposite 8-oxoG is general (the longer oligonucleotide system was also used to facilitate incorporation studies done at higher temperatures, see below). Analysis of the product indicated only incorporation of C and no A, G, or T (supplementary data Fig. 2S and Table 3S) (with the limit of detection realistically being 2–3%).

Pre-steady-state Kinetic Analysis of Insertion of dNTPs Opposite 8-OxoG—The steady-state analyses (see below) suggested that insertion of dCTP opposite 8-oxoG was as efficient as opposite G, but steady-state rates can be misleading in that they are often dominated by product off-rates (50). Pre-steady-state analysis of dCTP incorporation was done (Fig. 4). The preliminary results indicated that the initial rate of polymerization was at least as fast opposite 8-oxoG as opposite G, although the apparent steady-state rate was somewhat lower, as in the work presented in Table 2. With both G and 8-oxoG, the extent of the burst phase was quantitative with the Dpo4 concentration (estimated from UV analysis of the protein (37)). This result is only consistent with the rate-limiting step occurring after formation of the product (51, 52).

Further analysis was done using single turnover conditions, in which the concentration of Dpo4 was in excess of the oligonucleotide pair and the dNTP concentration was varied (52). The results (Fig. 5, A and B) were fit to hyperbolic plots (Fig. 5, C and D). For incorporation of dCTP opposite G, the values $k_{\text{pol}} = 1.1 \text{ s}^{-1}$ and $K_{d,\text{dCTP}} = 420 \mu\text{M}$ were estimated. For dCTP incorporation opposite 8-oxoG, the values $k_{\text{pol}} = 1.6 \text{ s}^{-1}$ and $K_{d,\text{dCTP}} = 27 \mu\text{M}$ were estimated (Fig. 5, B and D). Thus, incorporation of dCTP appears to be inherently more efficient opposite 8-oxoG than G.

Determination of E_a for dCTP Insertion Opposite G and 8-OxoG by Dpo4—The experiment shown in Fig. 4 was repeated at various temperatures in the presence of a high concentration of dCTP (Fig. 6). The assays were done at temperatures ranging from 20 to 50 °C using a longer oligonucleotide pair with a higher calculated T_m (68 °C) to facilitate the studies done at higher temperatures. This oligonucleotide pair (6:7, Scheme 1) had been analyzed for insertion preferences using MS

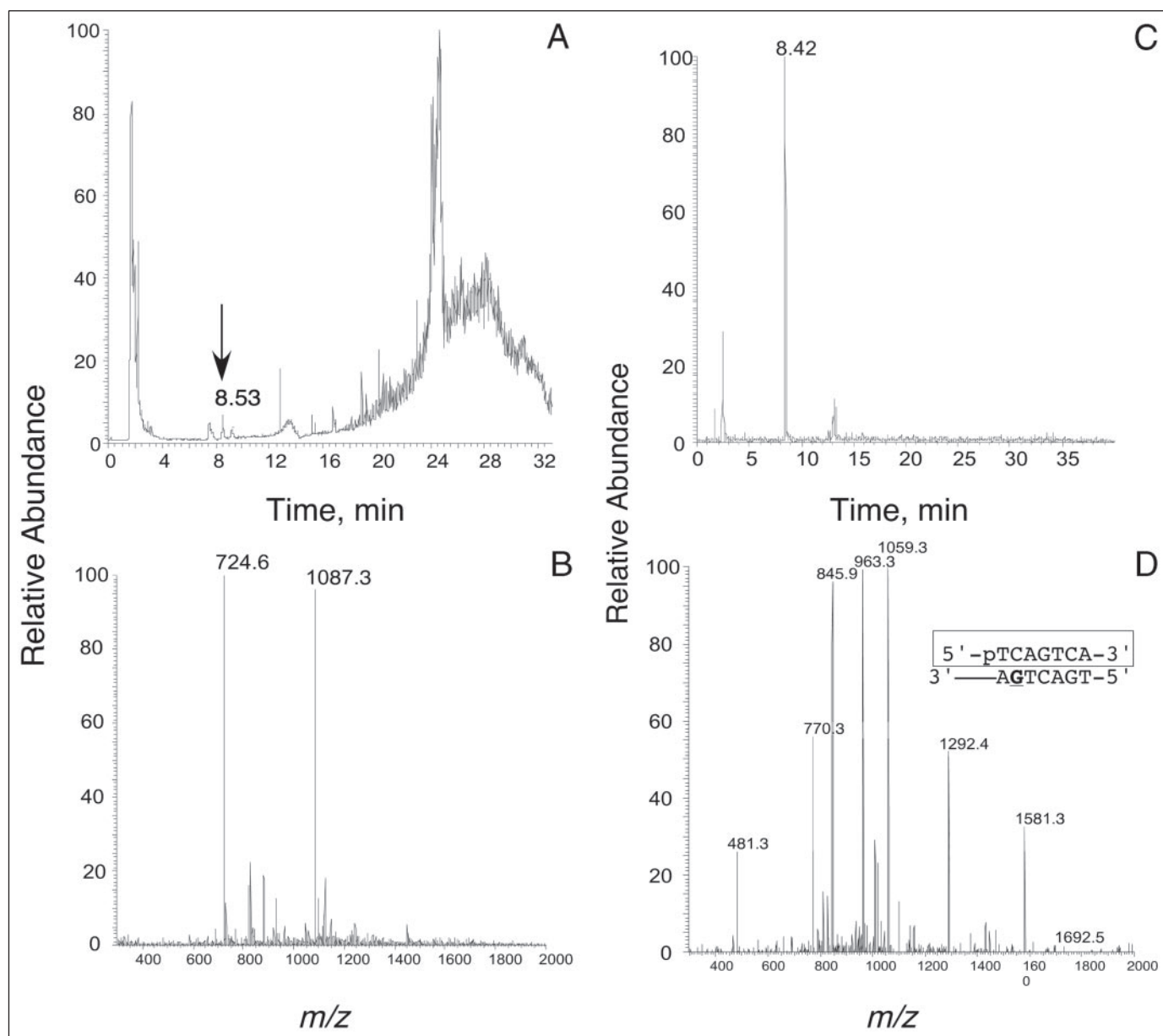


FIGURE 3. Analysis of Dpo4 reaction products by LC-MS/MS. *A*, total ion current trace of products derived from extension of oligomer **5** (paired opposite oligomer **2**). *B*, electrospray mass spectrum of the peaks eluted at 8.53 min. *C*, total ion current trace of ion m/z 1087.3. *D*, CID mass spectrum of ion m/z 1087.3 (from *B*). See also the supplemental data.

(supplementary data Fig. 2S). The results were fit to the Arrhenius equation $k_p = Ae^{-E_a/RT}$, where A is a reaction-specific constant, E_a is the activation energy, R is the gas constant ($1.99 \text{ cal deg}^{-1} \text{ mol}^{-1}$), and T is the absolute temperature (Fig. 7). The estimates of E_a for insertion opposite G and 8-oxoG were 8.4 and 4.2 kcal mol^{-1} , respectively.

Pre-steady-state Kinetic Analysis of Extension Beyond 8-OxoG Base Pairs—The steady-state kinetic analysis of the extension beyond 8-oxoG paired with A and C showed that extension beyond the 8-oxoG:C pair was preferred over the 8-oxoG:A pair, in contrast to all other polymerases examined (22–26, 33, 34) except yeast pol η (32). The system was examined using pre-steady-state kinetic analysis (Fig. 7). The k_p measured at a single high concentration of dGTP was 4-fold higher for insertion beyond the 8-oxoG:C pair than the 8-oxoG:A pair (Fig. 7). The k_p value for the 8-oxoG:C pair was even higher than for the corresponding G:C pair. The k_{ss} value for the 8-oxoG:C extension was less than for the other two oligonucleotides examined.

X-ray Crystal Structures of Dpo4 Complexes—To gain insight into the pairing modes of 8-oxoG at the active site of Dpo4 and potentially elucidate the structural bases of the biochemical observations, we determined crystal structures of five ternary Dpo4-DNA-(d)NTP complexes at resolutions between 2.27 and 2.6 Å. All crystals were obtained in the presence of Ca^{2+} , and potential traces of Mg^{2+} were masked with EDTA. Thus, the polymerase was expected to be inactive under the crystallization conditions used, as Ca^{2+} is a known inhibitor of DNA polymerases (53–56). To grow crystals of ternary complexes we used the 18-mer template **2**, modified with 8-oxoG (Scheme 1) (37), and the native DNA primer **1** (13-mer, Scheme 1). Both 2'-deoxyribonucleoside (dNTPs) and 2',3'-dideoxyribonucleoside triphosphates (ddNTPs) were co-crystallized with Dpo4 and the template-primer duplex. In previous crystallization experiments with Dpo4 complexes (37) we found that crystal quality often varied significantly, depending on whether dNTP or ddNTP was used for preparing the complex. The ddNTPs are

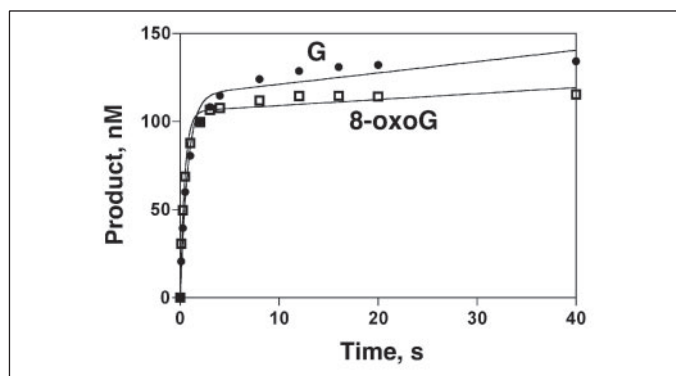


FIGURE 4. Pre-steady-kinetic course of insertion of dCTP opposite G and 8-oxoG. Oligomers **1** and **2** (Scheme 1) were used and the incorporation of dCTP opposite G (●) or 8-oxoG (□) was measured. The points were fit to plots with $k_p = 1.3 \text{ s}^{-1}$ and $k_{ss} = 0.0064 \text{ s}^{-1}$ for G and $k_p = 2.3 \text{ s}^{-1}$ and $k_{ss} = 0.0034 \text{ s}^{-1}$ for 8-oxoG. The concentrations of Dpo4, the primer-template complex, and dCTP were 100 nM, 200 nM, and 500 μM , respectively.

normally inhibitors of Dpo4 activity; thus, single extension of the primer by a ddNTP is much less efficient relative to the corresponding dNTP prevented even in the presence of Mg^{2+} and despite availability of a 3'-OH at the primer terminus (data not shown).

Crystals of the Dpo4-dGTP and Dpo4-ddGTP complexes (referred to here as Dpo4-dG and Dpo4-ddG, respectively) could be grown relatively easily, and the latter diffracts to higher resolution (Table 1). By comparison, the crystals of the Dpo4-dATP, Dpo4-dCTP, and Dpo4-ddCTP ternary complexes (referred to here as Dpo4-dA, Dpo4-dC, and Dpo4-ddC, respectively) often showed split reflections in diffraction frames or twinning that made indexing impossible. A large number of crystals of these complexes were screened to identify specimens suitable for structure determination and refinement (see the summary of crystal data and refinement parameters in Table 1). Examples for the quality of the final electron density for all five crystal structures are depicted in Fig. 8.

The Dpo4-dG and Dpo4-ddG complexes are of the Type II form (36), with two template bases lodged at the active site of the polymerase (8-oxoG and the 5' adjacent C, Fig. 8, A and D). Both structures display close similarity to the structure of the ternary complex with a DNA of identical sequence but with 1, N^2 -ethenoG in place of 8-oxoG (37), consistent with the straightforward phasing of the Dpo4-dG and -ddG structures via molecular replacement, using the 1, N^2 -ethenoG complex as the search model. The 8-oxoG is stacked inside the duplex but does not pair with the base from the incoming nucleoside triphosphate. Instead, the latter is inserted opposite the 5' adjacent template C, leaving a gap to the 3'-terminal primer base that is itself paired with the template G that follows 8-oxoG. The base moieties of (d)dGTP and the 3'-terminal cytidine in the primer are subtly tilted around 8-oxoG, thus reducing the distance between the terminal 3'-hydroxyl group of the primer and the α -phosphate group (Fig. 8, A and D). Conversely, the Dpo4-dA, -dC, and -ddC complexes belong to the Type I form (36), in which 8-oxoG of the template and nucleoside triphosphate constitute the single base pair at the active site (Fig. 8, B, C, and E).

The active site conformations classified as Types I and II represent only one difference between the Dpo4-dG and -ddG structures on the one hand and the Dpo4-dA, -dC, and -ddC structures on the other. Analysis of the latter structures revealed the presence of an additional nucleotide at or adjacent to the polymerase active site. In the Dpo4-dA structure, electron density is consistent with a second dATP molecule nested against the minor groove of the primer-template duplex, such that its triphosphate moiety is directed into the active site (Fig. 9A). The

nucleobase of the second dATP practically dissects the minor groove, but only a single hydrogen bond to a base from the template strand is formed (N-6 to O-2 of T-9, 3.41 Å). The 3'-OH of this dATP is hydrogen bonded to the side chain of Ser¹⁰³ and to the amide nitrogen from the same residue (Fig. 10B). The short distance (2.51 Å) between the terminal 3'-hydroxyl oxygen of the primer strand and the α -phosphorus of the second dATP indicates the possibility that a small fraction of the primer strand has actually been extended in the crystal structure. By comparison, the distance between the 3'-OH and the α -phosphorus of the dATP molecule located opposite 8-oxoG at the active site is much longer (6.51 Å; Fig. 9A).

In both the Dpo4-dC and -ddC structures, the electron density reveals 14-mer primers (13-mer **1**, Scheme 1, extended by a single C). The orientations of C14 in the two complexes are very similar to the nucleoside portion of dATP in the Dpo4-dA complex (Fig. 9). The contact between N-4 of C14 and O-2 of template T9 in Dpo4-dC is slightly long (3.95 Å). Instead hydrogen bonds now exist between the exocyclic amino group of C14 and O-2 of T11 from the primer and O-4' of the adjacent residue T12 (3.55 and 2.86 Å, respectively; Fig. 9B). The 3'-hydroxyl oxygen of C14 is hydrogen bonded to the backbone carbonyl oxygen of Ala¹⁰² (3.42 Å, Fig. 10C). However, because the backbone curls around between C13 and C14, the 3'-OH of C14 is far removed from the σ -phosphorus of the dCTP paired with 8-oxoG (10.1 Å, Fig. 10C).

The presence of a second dATP in the Dpo4-dA structure and extended primers in the Dpo4-dC and -ddC structures are accompanied by subtle rearrangements of the metal ions normally coordinated at and adjacent to the active site (Figs. 11 and 12). In some cases, additional ions are observed. Thus, in the Dpo4-dA complex, five Ca^{2+} ions stabilize the 8 total negative charges of the two dATP molecules and adjacent phosphates of the primer strand (Fig. 10B); in the Dpo4-ddC complex, four Ca^{2+} ions are located at the active site as compared with the three ions normally seen in Dpo4 binary and ternary complexes (37). Comparisons between the individual complex structures as well as between the structures of DNA duplexes in the Dpo4 complexes alone reveal various deviations (Figs. 11 and 12). In general, the r.m.s. deviations between superimposed $\text{C}\alpha$ atom positions for Type II complexes (Dpo4-dG, -ddG, and 1JXL (36)) are ~ 0.4 Å. For those between $\text{C}\alpha$ atoms of Type I complexes (Dpo4-dA, -dC, -ddC, and 1JX4 (36)) they are about 0.8 Å. From the illustrations in Figs. 11 and 12 it is also apparent that the orientation of the DNA primer-template duplex in the Dpo4-dG complex differs only minimally from the one in the complex with native DNA (Fig. 12A). However, the superimposed structures of Type I complexes show considerable deviations (Fig. 11) and the changes in DNA orientation seen in the Dpo4-dA complex relative to the reference structure (1JX4, Fig. 11B) somewhat exceed those found for the Dpo4-dC (Fig. 11C) and -ddC complexes (Fig. 11D). It is clear that these deviations are in part because of the presence of a second nucleoside triphosphate (Dpo4-dA) or the need to accommodate an extended primer (Dpo4-(d)dC).

The observation in the structures of Dpo4 activity with the 8-oxoG-modified template and either dCTP or ddCTP under the crystallization conditions used (*i.e.* in the absence of Mg^{2+}) is unexpected. We conducted single nucleotide extension experiments with the 13-mer primer **1** paired with 18-mer template **2** in the presence of Ca^{2+} and demonstrated that Dpo4 is indeed active with dCTP, ddCTP, and dATP, albeit much more slowly than with Mg^{2+} but at a rate significant enough for the time frame used for crystallization (data not shown). It is noteworthy in view of the more efficient incorporation opposite 8-oxoG of dCTP relative to dATP (Table 2) that it is the Dpo4-dC and -ddC com-

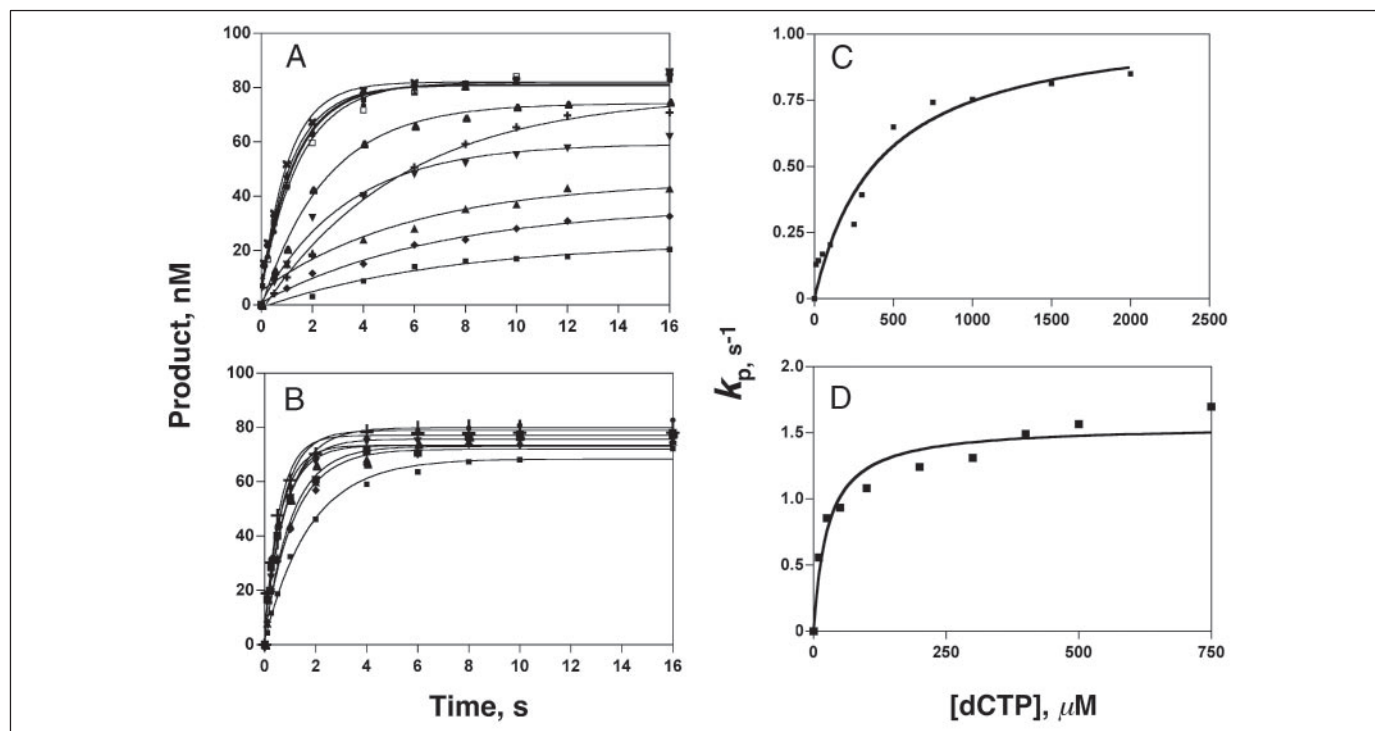


FIGURE 5. Determination of k_{pol} and $K_{\text{d,dCTP}}$ for incorporation of dCTP opposite G and 8-oxoG. A and B, the experiments shown in Fig. 4 were repeated at varying concentrations of dCTP with incorporation opposite G (A) or 8-oxoG (B). C and D, the values of k_p estimated in A and B were plotted versus [dCTP]. C, for incorporation opposite G, $k_{\text{pol}} = 1.1 \text{ s}^{-1}$ and $K_{\text{d,dCTP}} = 420 \text{ } \mu\text{M}$. D, for incorporation opposite 8-oxoG, $k_{\text{pol}} = 1.6 \text{ s}^{-1}$ and $K_{\text{d,dCTP}} = 27 \text{ } \mu\text{M}$.

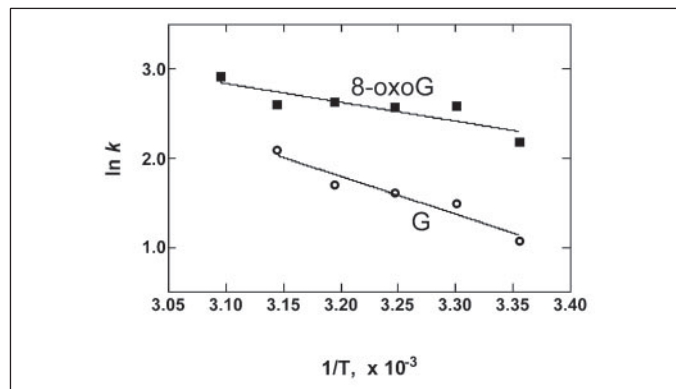


FIGURE 6. Activation energy for dCTP incorporation by Dpo4. k_p was measured using a dCTP concentration of $500 \text{ } \mu\text{M}$, with 50 nM Dpo4 and 200 nM primer-template complex (oligomer 6 paired with either oligomer 7, Scheme 1), with all measurements being made using a rapid quench apparatus. The temperature varied from 25 to $50 \text{ } ^\circ\text{C}$ (readings from a YSI thermocouple (Yellow Springs Instrument Co., Yellow Springs, OH) attached to the water bath compartment of the rapid quench apparatus). The resulting k_p rates were fit to the Arrhenius expression, $k_p = Ae^{-E_a/RT}$ (where A is a reaction-specific constant, E_a is the activation energy, R is the gas constant ($1.99 \text{ cal deg}^{-1} \text{ mol}^{-1}$), and T is the absolute temperature) to yield $E_a = 8.4 \pm 1.3$ and $4.2 \pm 1.2 \text{ kcal mol}^{-1}$ for dCTP incorporation opposite G and 8-oxoG, respectively.

plexes that exhibit primers extended by a single residue in the crystal structures. Moreover, the *in vitro* primer extension studies with individual dNTPs or ddNTPs and Ca^{2+} show that dCTP and ddCTP are inserted most efficiently opposite 8-oxoG (a more detailed discussion of these results and their correlation with the structures of Dpo4 complexes will be published elsewhere).

A fundamental difference between the Dpo4-(d)dc and Dpo4-dA complexes concerns the pairing mode of the respective nucleoside triphosphates with 8-oxoG (Fig. 10). In the Dpo4-dC and -ddC complexes, dCTP and 8-oxoG pair in a standard Watson-Crick fashion (Fig. 10C). However, at the active site of the Dpo4-dA complex, 8-oxoG

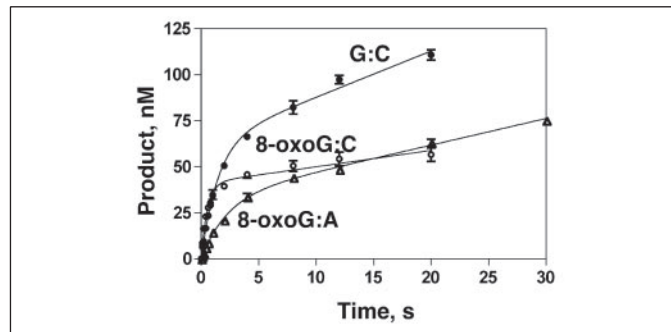


FIGURE 7. Pre-steady-state kinetic course of next base incorporation of dGTP opposite C by Dpo4 following various base pairs. Results are shown for incorporation following a G:C pair (●), 8-oxoG:C pair (○), or 8-oxoG:A pair (△) (G or 8-oxoG in template strand). The following parameters were estimated: G:C, $k_p = 0.69 \text{ s}^{-1}$ and $k_{\text{ss}} = 0.050 \text{ s}^{-1}$; 8-oxoG:C, $k_p = 1.9 \text{ s}^{-1}$ and $k_{\text{ss}} = 0.018 \text{ s}^{-1}$; 8-oxoG:A, $k_p = 0.45 \text{ s}^{-1}$ and $k_{\text{ss}} = 0.030 \text{ s}^{-1}$. The concentration of Dpo4, primer-template complex, and dCTP were 50 nM , 150 nM , and $500 \text{ } \mu\text{M}$, respectively.

assumes a *syn* conformation and pairs with dATP in a Hoogsteen fashion (Fig. 10B). This conformational switch of 8-oxoG triggers an important change in terms of its interaction with Arg³³² from the little finger domain. In the Dpo4-dC complex, the guanidinium moiety of Arg³³² is engaged in a hydrogen bond to O-8 of 8-oxoG in addition to stabilizing the template backbone (distance $3.19 \text{ } \text{Å}$; Fig. 10C). The *syn* conformation of 8-oxoG in Dpo4-dA leads to disruption of this hydrogen bond (the distance between Arg and N-3 of 8-oxoG is $4.26 \text{ } \text{Å}$; Fig. 10B). The above direct contact between a Dpo4 side chain and 8-oxoG is unique and clearly absent in the structures of complexes with native DNA (36). In the Dpo4-dG complex, Arg³³² forms hydrogen bonds to both the phosphate of the C 5' adjacent to 8-oxoG, as well as to O-8 of 8-oxoG (Fig. 10A). The non-sequence specific interaction with the phosphate backbone of the template strand corresponds most likely to the role played by Arg³³² in the replication of native DNA. For now we note that

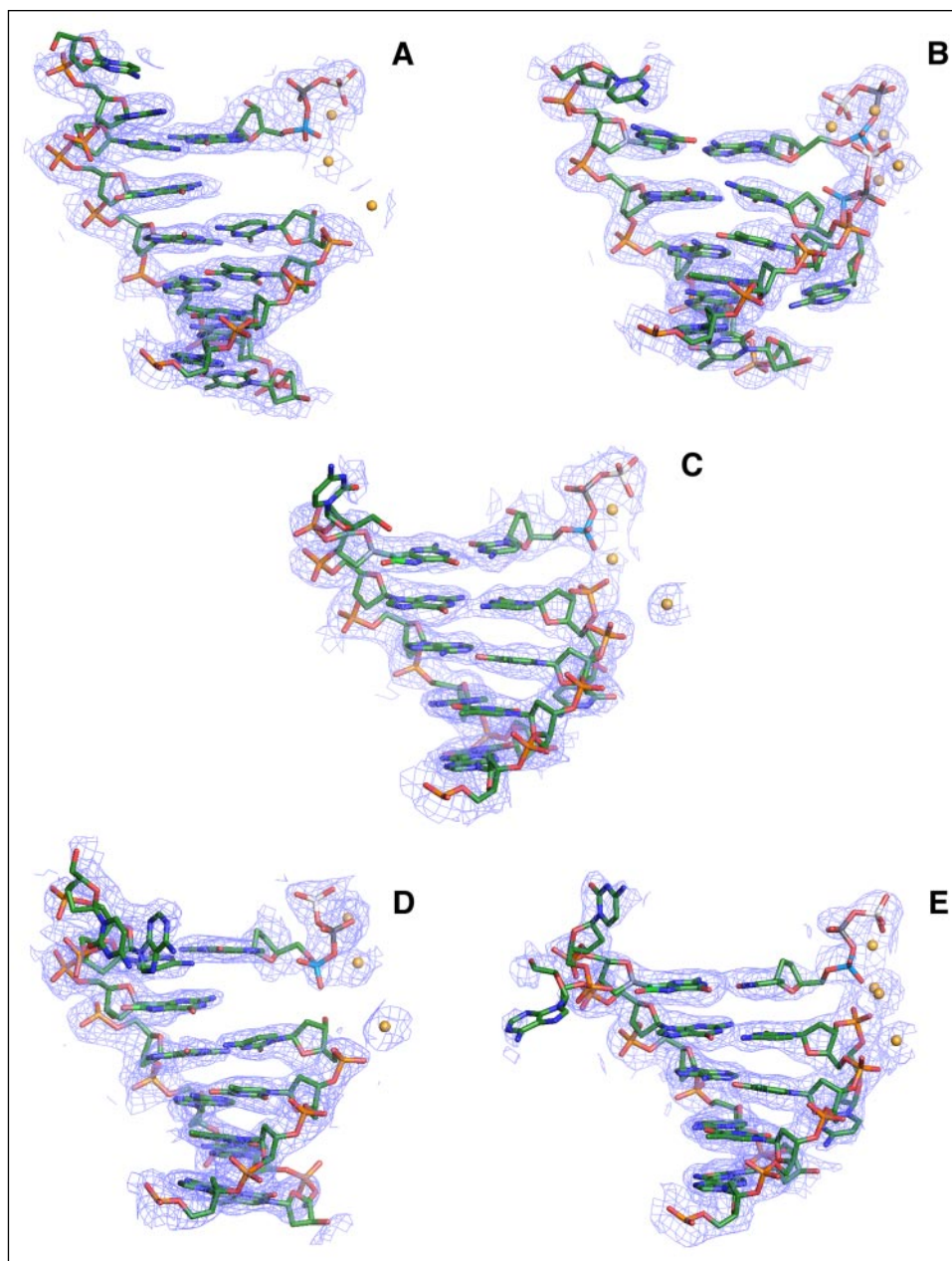


FIGURE 8. Quality of the electron density and DNA duplex conformations at the active sites in the ternary complexes. A, Dpo4-dG; B, Dpo4-dA; C, Dpo4-dC; D, Dpo4-ddG; E, Dpo4-ddC. The views are into the major groove, Fourier ($3F_o - 2F_c$) sum electron density is drawn at the 1σ level, Ca^{2+} ions are *yellow spheres*, and phosphorus atoms of the α -, β -, and γ -phosphate groups of (d)NTPs are highlighted in *cyan, gray, and white*, respectively.

the hydrogen bond observed between Arg³³² and the O-8 carbonyl oxygen of 8-oxoG, with an *anti* orientation, will undoubtedly influence the efficiencies with which either dCTP or dATP are inserted opposite 8-oxoG. In addition, this interaction should also affect the relative binding strength of dCTP to G and 8-oxoG.

DISCUSSION

Dpo4 is an interesting polymerase in that this enzyme catalyzes the preferential incorporation of dCTP opposite the common DNA oxidation product 8-oxoG, instead of dATP. The preferential incorporation of C was established using LC-MS/MS analysis with the products derived from two different oligonucleotide sequences (Fig. 3 and supplementary data Fig. 2S). Dpo4 was even more efficient in inserting dCTP opposite 8-oxoG than opposite G, as judged by steady-state and pre-steady-state kinetic analysis. The E_a value for insertion of dCTP opposite 8-oxoG was more favorable than opposite G. Furthermore, the efficiency of extension beyond an 8-oxoG:C pair was similar to that for

a G:C pair in the sequence examined and ~ 4 -fold more efficient (k_{cat}/K_m) than for an 8-oxoG:A pair. Analysis of the crystal structures shows that, in contrast to the normal Watson-Crick base pairing and geometry, the interaction of A with a template 8-oxoG has the 8-oxoG in the abnormal *syn* conformation and the A in the normal *anti* configuration (Fig. 10). In a crystal containing dGTP, a very unfavorable substrate, the G was paired not with the adduct (8-oxoG) but with the 5' base of the adduct in the template (C), a phenomenon seen with Dpo4 and some other DNA adducts (37, 47).

The results of the LC-MS/MS analysis (Fig. 3 and supplementary data) of the products of the Dpo4-catalyzed polymerization of the oligonucleotide pair 5:2 (Scheme 1, Fig. 1) are semi-quantitatively consistent with the results of the steady-state (Fig. 2, Table 2) and pre-steady-state (Figs. 5 and 6) kinetic assays, in that incorporation of C is observed in $\sim 95\%$ of the events and insertion and extension beyond A are observed the remainder of the time. The incorporation of dCTP \gg dATP was also observed in another sequence context using LC-MS/MS

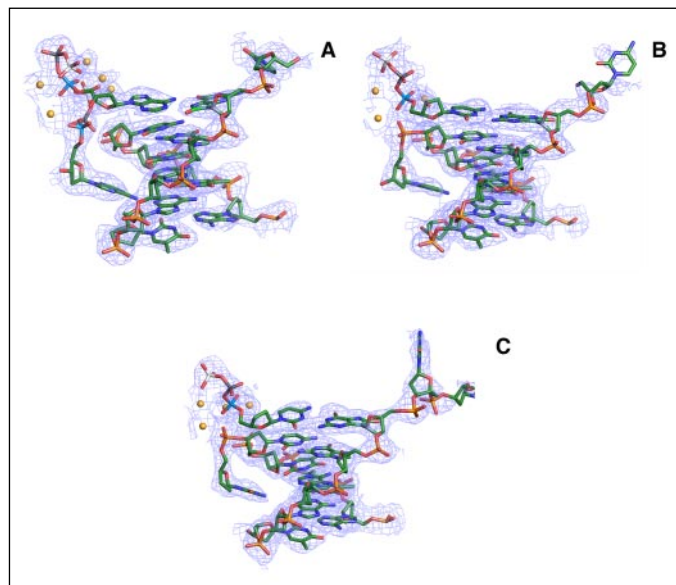


FIGURE 9. Orientations of the second nucleoside triphosphate molecule and the 3'-terminal, 14th nucleotide at the active sites of the Dpo4-dATP and Dpo4-(d)dCTP complexes, respectively. A, Dpo4-dA; B, Dpo4-dC; C, Dpo4-ddC. Sum of the electron density is drawn as described in the legend to Fig. 8 and the DNAs rotated around the vertical by $\sim 180^\circ$ compared with Fig. 8, such that the views are in the minor groove.

analysis (supplementary data Fig. 2S) and is not considered to be a sequence-specific phenomenon.

DNA polymerases vary considerably in their tendencies to insert dCTP or dATP opposite a template 8-oxoG in single nucleotide misincorporation assays, with most preferring to insert dATP. For example, the thermophilic bacterial replicative pol BF (27) and human immunodeficiency virus type 1 reverse transcriptase (24) insert dATP in $\geq 90\%$ of the incorporation events in the oligonucleotides examined. Of the other studies available with various polymerases, including bovine pols α and δ , *E. coli* pols I (Klenow fragment) and II (exo^-), yeast pol η , bacteriophage pol T7, and pols BF and RB69 (22–27, 29, 30, 34, 57), the ratio of dATP:dCTP incorporation varies (21) and only Dpo4 (this work) and yeast (and probably human) pol η (32) have been found to preferentially extend 8-oxoG:C pairs relative to 8-oxoG:A pairs. It is of interest to contrast this behavior of Dpo4 in placing dCTP opposite template 8-oxoG with the report of the same enzyme to exclusively insert 8-oxo dGTP opposite template A, instead of C (58). These latter results, reminiscent of the reported asymmetry of the 8-oxoG pairs demonstrated earlier with other polymerases (25), clearly show that the patterns cannot be explained only in the context of strength of base pairing. The only two DNA polymerases that had been reported to show a high tendency to insert dCTP opposite 8-oxoG, instead of dATP, are RB69 (26) and *S. cerevisiae* pol η (30, 32). These enzymes insert dATP in only $\sim 5\%$ of the incorporation events, as judged by the available data. Dpo4 yields a similar value of $\sim 2\%$ (Table 2, Fig. 3, and supplemental data). In the case of RB69, a crystal structure is available with dCTP bound, but not with dATP (26). No structure is available for the yeast pol η complex; pre-steady-state kinetic measurements indicate the same K_d for dATP as for dCTP, with the difference being in the k_{pol} (30). In our own work, the K_d for dCTP binding opposite 8-oxoG was considerably lower than opposite G, an unexpected result (Fig. 5).

Even with a model DNA polymerase such as Dpo4, the mechanisms underlying discrimination of nucleotides and appropriate pairing are still the source of investigation and discussion (35). Possible mechanisms include optimization base stacking and metal alignment and

coordination. The new structural data sheds light on the above observations regarding 8-oxoG. In the Dpo4-dC complex (the situation in Dpo4-ddC is similar), Arg³³² is hydrogen bonded to O-8 of 8-oxoG (Fig. 10C). In Dpo4-dA where 8-oxoG adopts a *syn* conformation, formation of this hydrogen bond is prevented as O-8 is now rotated away from the border of the major groove into the minor groove and N-3 is too far away to allow interaction with Arg³³² (Fig. 10B). The existence of this hydrogen bond has important consequences for the relative efficiencies of dCTP and dATP insertion opposite a template 8-oxoG because it changes the energetics of the *syn/anti* equilibrium in 8-oxoG. The *anti* conformation of 8-oxoG is accompanied by sterically unfavorable contacts between the 8-oxygen and the deoxyribose moiety. The *syn* orientation of the nucleobase becomes more favorable in 8-oxoG compared with G because it relieves the steric strain, hence the preferred incorporation of dATP in the Hoogsteen mode opposite 8-oxoG by the majority of polymerases including most Y-class polymerases. Likewise, incorporation of 8-oxo dGTP is strongly preferred opposite template-A by all polymerases including Dpo4. Obviously, the interaction between Arg³³² and O-8 will shift the *syn/anti* equilibrium for 8-oxoG in the template toward the *anti* conformation. Instead of the Hoogsteen face, 8-oxoG will normally present its Watson-Crick face to the nucleoside triphosphate at the active site of Dpo4 and thus pair preferably with dCTP. Conversely, 8-oxo-dGTP is expected to adopt a *syn* conformation in Dpo4 and pair with template A in the Hoogsteen mode. The apparent contradiction constituted by deviating pairing modes of 8-oxoG in the template and as a nucleotide substrate of Dpo4 can therefore be fully resolved thanks to the structural data.

The interaction between Arg³³² and 8-oxoG in the DNA template is unique, first because none of the four natural bases features an acceptor functionality at the edge of the major groove and, second, because the little finger domains (residues 244–341 in *Sulfolobus solfataricus* Dpo4) exhibit a high degree of sequence diversity. Judging from a structure-based sequence alignment (36), *E. coli* UmuC (pol V), *E. coli* DinB (pol IV), human pol η (Rad30A), pol ι (Rad30B), and pol κ (DinB1), and *S. cerevisiae* pol η (Rad30) do not have an Arg in position 332. In both human pols κ and η , Arg³³² is replaced by His, but it is unlikely that His can engage in the same interaction as Arg at the active site of Dpo4.

Our crystal structures of Dpo4 complexes with DNA templates containing 8-oxoG may also provide a rationalization of the preferential extension of 8-oxoG:C pairs relative to 8-oxoG:A pairs. In the Type II structure found for the Dpo4-dG complex, Arg³³² also forms a hydrogen bond to O-8 of 8-oxoG (Fig. 10A), although the template base is shifted down relative to its position in the Dpo4-dA and -dC complexes (Fig. 10, B and C, respectively). Thus, Arg³³² is capable of slightly changing its orientation and interacts with an 8-oxoG that is being replicated and also with one that has moved to the -1 position following strand relocation. In both orientations, the side chain will afford stabilizing interactions with backbone phosphates (Fig. 10). As is the case for the corresponding pair in a replicating mode, the *syn* 8-oxoG:A pair, now shifted down by a single step, cannot interact with Arg³³² via O-8. The conservation of this interaction with 8-oxoG during and after replication most likely stabilizes local conformation and orientation of the template-primer duplex and may thus contribute favorably to the extension of the 8-oxoG:C pair compared with that of the 8-oxoG:A pair.

The catalytic efficiency (as reflected in the steady-state parameter k_{cat}/K_m) for insertion of dCTP opposite 8-oxoG is similar to that opposite G (Table 2). The steady-state K_m for the 8-oxoG reaction was 6-fold lower, and the k_{cat} was about $1/3$ that for insertion of dCTP opposite G (Table 2, Fig. 2, top panel). A similar pattern was observed for the steady-state kinetics of extension beyond 8-oxoG:C versus a G:C pair

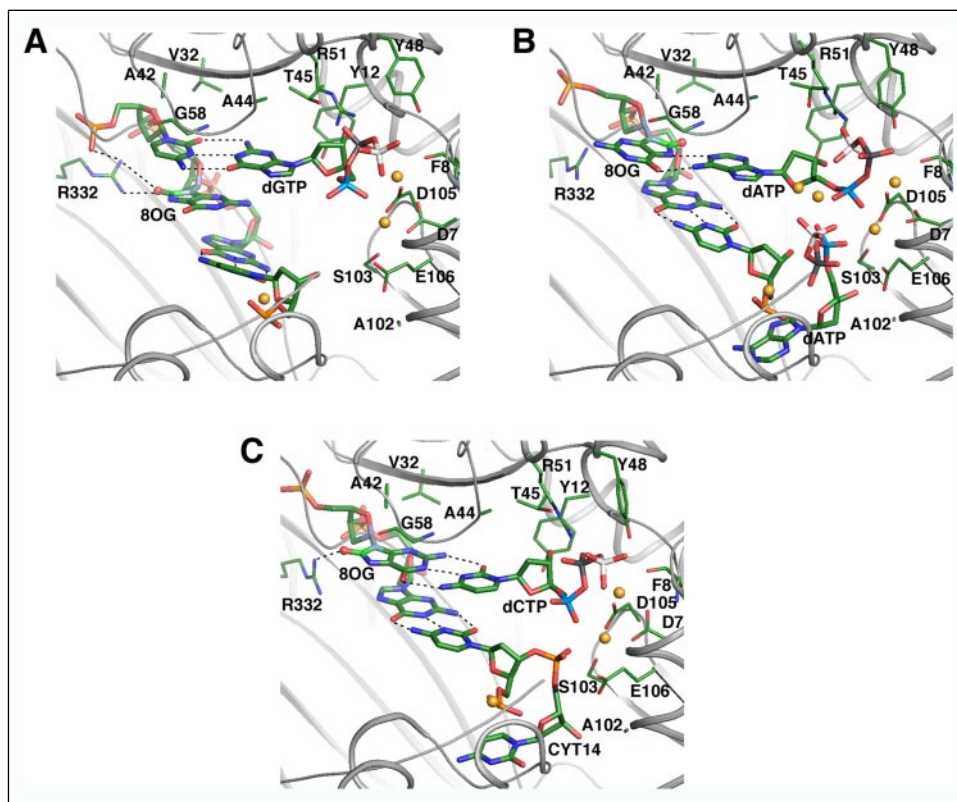


FIGURE 10. Base pairing modes of 8-oxoG (8OG) at the active sites of the Dpo4-dGTP, -dATP, and -dCTP complexes. A, Dpo4-dG; B, Dpo4-dA; C, Dpo4-dC. DNA base pairs are colored by the atom, Ca^{2+} ions are yellow spheres, and hydrogen bonds are dashed lines. The Ca backbone of the polymerase is shown in schematic form, with selected side chains added and labeled.

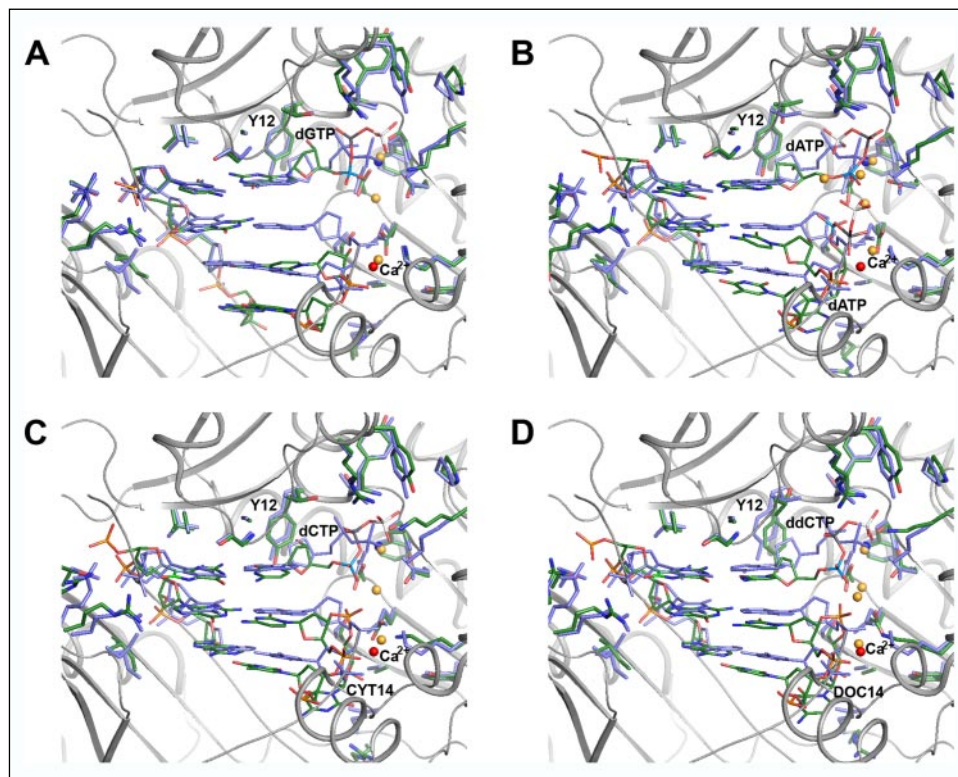
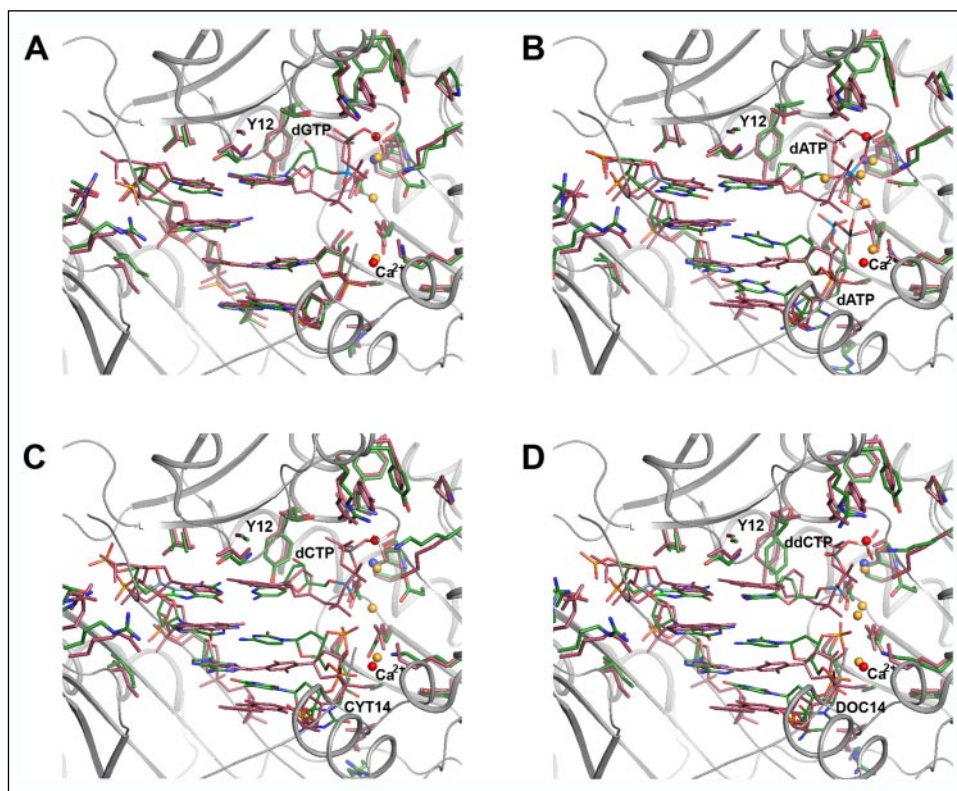


FIGURE 11. Comparisons between the structures of Dpo4 ternary complexes containing 8-oxoG-modified DNA with the Type I Dpo4-DNA-ddATP complex (36). A, Dpo4-dG; B, Dpo4-dA; C, Dpo4-dC; D, Dpo4-ddC. The DNA in the 8-oxoG complexes is colored by the atom and Ca^{2+} ions are yellow spheres. The DNA in the ternary complex with native DNA (PDB code 1JX4) is colored blue and the Ca^{2+} and Mg^{2+} ions are blue and red spheres, respectively. The Ca backbone of the polymerase is shown in schematic form and selected side chains have been added for comparison, with the coloring matching that of the DNA in the respective structures. CYT, 2',3'-dideoxycytidine.

(Table 2). The basis for these results is not clear, in that the exact meaning of steady-state kinetic parameters in DNA polymerase reactions is not very obvious (50). These results are consistent with the differences in the k_{ss} component in the pre-steady-state kinetic assays, as might be expected (Figs. 4 and 5). One result that is rather striking is the much

lower $K_{d,dCTP}$ value measured for incorporation opposite 8-oxoG (27 μM) versus G (420 μM) (Fig. 5, C and D). In principle, this value, determined using single-turnover conditions (Fig. 5, A and B), should reflect the dissociation constant for the substrate dCTP in the enzyme intermediate poised for phosphodiester bond formation (52).

FIGURE 12. Comparisons between the structures of Dpo4 ternary complexes containing 8-oxoG-modified DNA with the Type II Dpo4-DNA-ddGTP complex (36). A, Dpo4-dG; B, Dpo4-dA; C, Dpo4-dC; D, Dpo4-ddC. The DNA in the 8-oxoG complexes is colored by the atom and Ca^{2+} ions are yellow spheres. The DNA in the ternary complex with native DNA (PDB code 1JXL) is colored in red and Ca^{2+} and Mg^{2+} ions are blue and red spheres, respectively. The α backbone of the polymerase is shown in schematic form and selected side chains have been added for comparison, their coloring matching that of the DNA in the respective structures. CYT, 2'-deoxycytidine; DOC, 2',3'-dideoxycytidine.



The E_a , reflective of the transition state barrier, was more favorable for 8-oxoG than G in the system (Fig. 6). The kinetic burst observed in the pre-steady-state kinetics (Fig. 4) indicates that a step following product formation should be rate-limiting (Table 2, Fig. 4). One possibility we considered is that the k_{cat} (and k_{ss}) reflects the dissociation rate of the Dpo4-oligonucleotide complex. However, the rates were estimated using a carrier oligonucleotide trapping method (59–62) and found to be identical to each other and to the k_{ss} value measured for incorporation opposite G in the pre-steady-state experiments ($0.069 \pm 0.012 \text{ s}^{-1}$, results not shown). Thus we conclude that the off-rate for dissociation of the polymerase-oligonucleotide complex is not the basis of the K_d and K_m differences. (The point should also be made that dissociation of the Dpo4-oligonucleotide complex is a relatively slow process, and the distributive nature of the polymerase Dpo4, which is the result of a low ratio of $k_{\text{pol}}/k_{\text{off}}$ is attributed to the low k_{pol} rate more than to a high k_{off} rate.)

The crystal structures provide some insight into the mechanisms used by this enzyme, particularly in regards to the favorable transition state barrier for insertion of dCTP opposite 8-oxoG relative to G. Formation of the fortuitous hydrogen bond between Arg³³² and O-8 of 8-oxoG more or less freezes the template nucleoside in the *anti* conformation. Therefore, this interaction stabilizes the orientation of the template base at the active site. A more rigid template base is consistent with facilitated pairing to the substrate and a lower activation energy as long as it supports a geometry that is conducive to phosphodiester bond formation. Whether the Arg³³²-8-oxoG interaction explains the tighter binding between 8-oxoG and dCTP compared with the G:dCTP pair is more difficult to answer at this point, although the hypothesis can be tested. The presence of the carbonyl group at position 8 of G not only changes the N-7 atom from a hydrogen bond acceptor to a donor, but has additional stereoelectronic effects that influence nucleoside conformation and Watson-Crick hydrogen bonding strengths. Modulation of these effects by strong hydrogen bonds between O-8 and Arg may con-

tribute to the higher stability of the 8-oxoG:dCTP pair at the Dpo4 active site.

The crystal structures of the ternary Dpo4-dA and Dpo4-(d)dC complexes reported here are unusual in that they unexpectedly reveal additional nucleotides near the active site. In the case of Dpo4-dA, a second dATP molecule is lodged in the minor groove of the template-primer duplex in the immediate vicinity of the substrate dATP opposite 8-oxoG (Figs. 9A and 10B). In the Dpo4-dC and -ddC complexes the 13-mer primers were extended by a single C under the crystallization conditions used (Fig. 9, B and C). However, in both structures the primer strand turns sharply between C13 and C14 and thus allows accommodation of dCTP (or ddCTP) opposite 8-oxoG. Therefore, these complexes represent mixed substrate-product complexes and they demonstrate that Dpo4 may even be capable of carrying out two insertions opposite the same template base (8-oxoG in our case). Such behavior is consistent with a product isolated from *in vitro* primer extension reactions opposite a template with a single 1,*N*²-ethenoG adduct that can be explained by Dpo4 consecutively inserting two Ts opposite the same template A (37). The crystal structures of the Dpo4-dC and -ddC complexes indicate that the primer strand may bulge out into the minor groove prior to addition of the next nucleotide and that the channel formed by Dpo4 around the primer-template duplex provides enough space to tolerate the bulge. The disruption of the 8-oxoG:C pair at the active site and the looped-out conformation of (d)dC that allows binding of another (d)dCTP opposite the lesion is most likely the result of the particular metal ion (Ca^{2+}) used in the crystallization. However, the observed interaction between Arg³³² and O-8 of 8-oxoG in the *anti* conformation and the conclusions regarding its roles in the efficient insertion of dCTP opposite 8-oxoG and the asymmetry of the efficiency of incorporation (mostly insertion of 8-oxo dGTP opposite template dA versus mostly insertion of dCTP opposite template 8-oxo dG) is independent of the nature of the divalent metal ion. We will report details of the differences

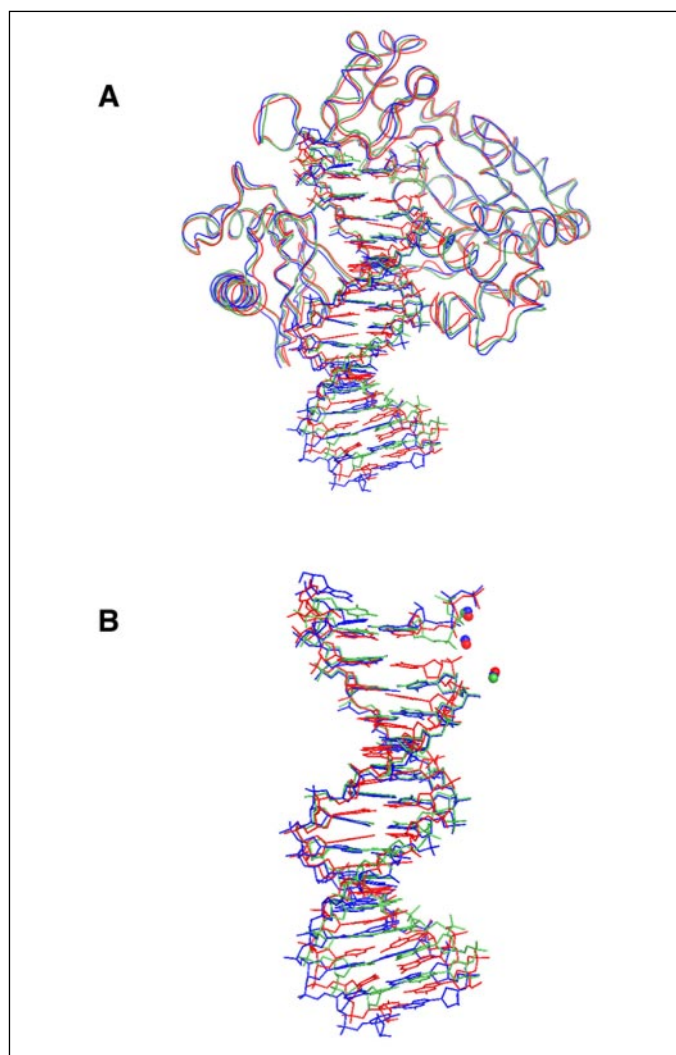


FIGURE 13. Comparison of polymerase and DNA conformations in Dpo4 ternary complexes with native and 8-oxoG-modified DNA template strands. *A*, overall conformations of the complexes; *B*, DNA conformations. The Dpo4-ddG and -dC complexes are colored in blue and red, respectively, and the Type I Dpo4-DNA-ddGTP ternary complex with native DNA (36) (PDB code 1JXL) is colored in green.

between Mg^{2+} and Ca^{2+} as cofactors of Dpo4 in a forthcoming manuscript.³

The Dpo4-dA, -dC, and -ddC complexes show significant deviations in terms of orientations of their DNA duplexes compared with the structures of the Dpo4-dG and -ddG complexes and those of ternary Dpo4 complexes with native DNA (36) (Figs. 11 and 12). When the structures of the entire complexes for Dpo4-ddG and Dpo4-dC and the Type II complex with native DNA (PDB ID code 1JXL) are superimposed, additional changes besides those regarding the DNA in the thumb and little finger domains of the protein become apparent (Fig. 13). Whereas the DNA and protein conformations in Dpo4-ddG and 1JXL are very similar (the duplex in the latter complex is shorter by one base pair), the Dpo4-dC complex exhibits larger changes in the conformation and orientation of the DNA and parts of the polymerase. The deviations in the case of the Dpo4-dA complex somewhat exceed those seen with Dpo4-dC. Although some of these structural changes are undoubtedly because of the additional nucleotides at the active sites of the Dpo4-dA and Dpo4-(d)dC complexes, the conformational vari-

ations in the polymerase, in particular those concerning the little finger domain, are noteworthy. The orientations of the little finger domain and the DNA duplex relative to the active site are of crucial importance for fidelity and processivity. The observation of product complexes for dCTP and ddCTP as opposed to the presence of a second dATP adjacent to the active site in the Dpo4-dA complex is fully consistent with the higher efficiency with which dCTP is incorporated opposite 8-oxoG relative to dATP.

Comparisons of the structural features with those of the four other published polymerase structures of 8-oxoG-containing oligonucleotides reveal some variation in modes of handling this adduct. Krahn *et al.* (28) reported structures of human pol β with dCTP and dAMP paired with template 8-oxoG (an unexpected scenario for this enzyme, which generally uses base-gapped substrates derived from elimination of modified bases). Although incorporation of dATP is a fairly frequent process in this experimental context, the 8-oxoG was in the standard *anti* conformation and was hydrogen bonded to the (*anti*) dCTP in the usual Watson-Crick manner. However, the 5'-phosphate backbone of the incoming dCTP was flipped 180°. When dAMP was bound, the 8-oxoG was in the *syn* conformation and bound in a Hoogsteen pair with the (*anti*) dAMP (28).

In complexes seen with the pol A family RB69 polymerase, the ternary polymerase-8-oxoG-dCTP complex is almost identical to the normal G:C pair and explains the preponderance of C insertion (26). No complex with A was reported. A structure of bacteriophage pol T7 has also been reported with dCTP opposite template 8-oxoG (29). As with pol β , pol T7 inserts dCTP in $\sim 2/3$ of events and dATP in $\sim 1/3$. The O-8 oxygen of the 8-oxoG is tolerated by the strong kinking of the DNA template (which may be related to the low k_{pol} for insertion of dCTP opposite 8-oxoG relative to G (24)). An 8-oxoG:A binary complex (A in the primer) has a Hoogsteen pair for the 8-oxoG (*syn*):A (*anti*) system, similar to that observed in our work with Dpo4. Finally, the pol BF complex (27) also forms Watson-Crick 8-oxoG (*anti*):C (*anti*) and Hoogsteen 8-oxoG (*syn*):A (*anti*) base pairs. The preliminary kinetic results reported indicate that the latter is favored, in terms of rates of product formation (27).

Thus, the general pattern appears to be that 8-oxoG is *anti* when paired with C but *syn* when paired with A, as we report here for Dpo4. The same pattern has been observed in double-stranded DNA in the absence of polymerases, using NMR and x-ray methods (18–20). Thus, the studies of 8-oxoG-modified oligonucleotides in the absence of protein have been predictive, even if not directly addressing the proclivity for mispairing, which is strongly dictated by the polymerases. However, these structures apparently have limited predictive values as to which should be dominant in the context of enzymatic polymerization and the course of misincorporation events. What is unusual about the results of this work with Dpo4 is that the *anti* 8-oxoG:*anti* C Watson-Crick pair is processed as efficiently or better than a G:C pair (and in preference to the 8-oxoG:A pair).

The structure of the 8-oxoG:C and 8-oxoG:A pairs seems to be rather constant in the different settings but does not predict fidelity, in the sense that the ratio of dCTP:dATP incorporation varies widely among the polymerases. Dpo4 appears to have the unusual ability of using an Arg from its little finger domain to set the 8-oxoG in the *anti* conformation and thus dictate pairing to an incoming dCTP. It is unclear whether there are other polymerases that rely on a similar mechanism or whether most adjust the 8-oxoG conformation *after* sensing the pairing of the system. Pre-steady-state kinetic parameters have been determined for dCTP incorporation opposite 8-oxoG with some of the polymerases. Values of $k_{pol} = 2-8 s^{-1}$ for Dpo4, depending on the sequence (this work), can be compared with $1.6-12 s^{-1}$ for pol T7 (24, 33), $22 s^{-1}$ for a bovine pol δ -proliferating cell nuclear antigen complex (34), and $2.2 s^{-1}$ for yeast pol η (30) (the $K_{d,dCTP}$ values range from 7 to 75 μM but

³ A. Irimia, H. Zang, L. V. Loukachevitch, F. P. Guengerich, and M. Egli, manuscript in preparation.

dNTP Incorporation Opposite 8-OxoG by Pol Dpo4

no clear pattern emerges). The k_{pol} and $K_{d,\text{dATP}}$ values have also been measured in several cases but no clear pattern emerges of why some polymerases have more fidelity. Although Dpo4 is often considered to be a prokaryotic model for the eukaryotic pol η , some distinct differences have been observed, e.g. in the case of bypass beyond another adduct, *cis-syn* thymine dimer (63).

In conclusion, the translesion polymerase Dpo4 copies past 8-oxoG with several interesting features. The reaction is relatively high fidelity, although not so much as the normal insertion opposite G. However, the catalytic efficiency of insertion of dCTP opposite 8-oxoG was at least as good or better than opposite G. This ease of insertion and the preference for incorporation of C and extending beyond it were unexpected. The crystal structures of ternary complexes are consistent with the ease of dCTP insertion in this system, and the structures reveal a hydrogen bond between Arg³³² from the little finger domain of Dpo4 and O-8 of the template 8-oxoG that may be key to the different performance of Dpo4 compared with some other DNA polymerases that have much less fidelity.

Acknowledgments—We thank L. Manier for assistance with the MS experiments, T. Iverson, Z. Wawrzak, and B. Zhao for help with x-ray data collection, and K. Trisler for assistance in preparation of the manuscript.

REFERENCES

1. Miller, J. A. (1998) *Drug Metab. Rev.* **30**, 645–674
2. Guengerich, F. P. (2001) *Mutat. Res.* **488**, 195–209
3. Friedberg, E., Walker, G. C., and Siede, W. (1995) *DNA Repair and Mutagenesis*, American Society of Microbiology, Washington, D. C.
4. Kornberg, A., and Baker, T. A. (1992) *DNA Replication*, 2nd Ed., W. H. Freeman, New York
5. Bauer, K. H. (1928) *Mutationstheorie der Geschwulstentstehung*, Springer, Berlin
6. Ames, B. N. (1979) *Science* **204**, 587–593
7. Shigenaga, M. K., Gimeno, C. J., and Ames, B. N. (1989) *Proc. Natl. Acad. Sci. U. S. A.* **86**, 9697–9701
8. Ravanat, J. L., Gremaud, E., Markovic, J., and Turesky, R. J. (1998) *Anal. Biochem.* **260**, 30–37
9. Malins, D. C., and Haimanot, R. (1991) *Cancer Res.* **51**, 5430–5432
10. Degan, P., Shigenaga, M. K., Park, E. M., Alperin, P. E., and Ames, B. N. (1991) *Carcinogenesis* **12**, 865–871
11. Fraga, C. G., Shigenaga, M. K., Park, J. W., Degan, P., and Ames, B. N. (1990) *Proc. Natl. Acad. Sci. U. S. A.* **87**, 4533–4537
12. Fraga, C. G., Motchnik, P. A., Shigenaga, M. K., Helbock, H. J., Jacob, R. A., and Ames, B. N. (1991) *Proc. Natl. Acad. Sci. U. S. A.* **88**, 11003–11006
13. Shimoda, R., Nagashima, M., Sakamoto, M., Yamaguchi, N., Hirohashi, S., Yokota, J., and Kasai, H. (1994) *Cancer Res.* **54**, 3171–3172
14. Henderson, P. T., Delaney, J. C., Muller, J. G., Neeley, W. L., Tannenbaum, S. R., Burrows, C. J., and Essigmann, J. M. (2003) *Biochemistry* **42**, 9257–9262
15. Neeley, W. L., Delaney, J. C., Henderson, P. T., and Essigmann, J. M. (2004) *J. Biol. Chem.* **279**, 43568–43573
16. Hailer, M. K., Slade, P. G., Martin, B. D., and Sugden, K. D. (2005) *Chem. Res. Toxicol.* **18**, 1378–1383
17. Culp, S. J., Cho, B. P., Kadlubar, F. F., and Evans, F. E. (1989) *Chem. Res. Toxicol.* **2**, 416–422
18. McAuley-Hecht, K. E., Leonard, G. A., Gibson, N. J., Thomson, J. B., Watson, W. P., Hunter, W. N., and Brown, T. (1994) *Biochemistry* **33**, 10266–10270
19. Kouchakdjian, M., Bodepudi, V., Shibutani, S., Eisenberg, M., Johnson, F., Grollman, A. P., and Patel, D. J. (1991) *Biochemistry* **30**, 1403–1412
20. Lipscomb, L. A., Peek, M. E., Morningstar, M. L., Verghis, S. M., Miller, E. M., Rich, A., Essigmann, J. M., and Williams, L. D. (1995) *Proc. Natl. Acad. Sci. U. S. A.* **92**, 719–723
21. Hogg, M., Wallace, S. S., and Doublet, S. (2005) *Curr. Opin. Struct. Biol.* **15**, 86–93
22. Shibutani, S., Takeshita, M., and Grollman, A. P. (1991) *Nature* **349**, 431–434
23. Lowe, L. G., and Guengerich, F. P. (1996) *Biochemistry* **35**, 9840–9849
24. Furge, L. L., and Guengerich, F. P. (1997) *Biochemistry* **36**, 6475–6487
25. Einolf, H. J., Schnetz-Boutaud, N., and Guengerich, F. P. (1998) *Biochemistry* **37**, 13300–13312
26. Freisinger, E., Grollman, A. P., Miller, H., and Kisker, C. (2004) *EMBO J.* **23**, 1494–1505
27. Hsu, G. W., Ober, M., Carell, T., and Beese, L. S. (2004) *Nature* **431**, 217–221
28. Krahn, J. M., Beard, W. A., Miller, H., Grollman, A. P., and Wilson, S. H. (2003) *Structure (Camb.)* **11**, 121–127
29. Briebe, L. G., Eichman, B. F., Kokoska, R. J., Doublet, S., Kunkel, T. A., and Ellenberger, T. (2004) *EMBO J.* **23**, 3452–3461
30. Carlson, K. D., and Washington, M. T. (2005) *Mol. Cell. Biol.* **25**, 2169–2176
31. Einolf, H. J., and Guengerich, F. P. (2000) *J. Biol. Chem.* **275**, 16316–16322
32. Haracska, L., Yu, S. L., Johnson, R. E., Prakash, L., and Prakash, S. (2000) *Nat. Genet.* **25**, 458–461
33. Furge, L. L., and Guengerich, F. P. (1998) *Biochemistry* **37**, 3567–3574
34. Einolf, H. J., and Guengerich, F. P. (2001) *J. Biol. Chem.* **276**, 3764–3771
35. Vaisman, A., Ling, H., Woodgate, R., and Yang, W. (2005) *EMBO J.* **24**, 2957–2967
36. Ling, H., Boudsocq, F., Woodgate, R., and Yang, W. (2001) *Cell* **107**, 91–102
37. Zang, H., Goodenough, A. K., Choi, J.-Y., Irimia, A., Loukachevitch, L. V., Kozekov, I. D., Angel, K. C., Rizzo, C. J., Egli, M., and Guengerich, F. P. (2005) *J. Biol. Chem.* **280**, 29750–29764
38. Howard, A. J. (2000) *Crystallographic Computing 7: Proceedings from the Macromolecular Crystallographic Computing School* (Bourne, P. E., and Watenpaugh, K. D., eds) Oxford University Press, Oxford, UK
39. Kabsch, W. (1988) *J. Appl. Crystallogr.* **21**, 916–924
40. French, G. S., and Wilson, K. S. (1978) *Acta Crystallogr. Sect. A* **34**, 517–525
41. McCoy, A. J., Grosse-Kunstleve, R. W., Storoni, L. C., and Read, R. J. (2005) *Acta Crystallogr. D Biol. Crystallogr.* **61**, 458–464
42. Vellieux, F. M. D., and Dijkstra, B. W. (1997) *J. Appl. Crystallogr.* **30**, 396–399
43. Brünger, A. T., Adams, P. D., Clore, G. M., DeLano, W. L., Gros, P., Grosse-Kunstleve, R. W., Jiang, J. S., Kuszewski, J., Nilges, M., Pannu, N. S., Read, R. J., Rice, L. M., Simonson, T., and Warren, G. L. (1998) *Acta Crystallogr. D Biol. Crystallogr.* **54**, 905–921
44. Laskowski, L. A., MacArthur, M. W., Moss, D. S., and Thornton, J. M. (1999) *J. Appl. Crystallogr.* **26**, 283–291
45. Ling, H., Boudsocq, F., Plosky, B. S., Woodgate, R., and Yang, W. (2003) *Nature* **424**, 1083–1087
46. Ling, H., Sayer, J. M., Plosky, B. S., Yagi, H., Boudsocq, F., Woodgate, R., Jerina, D. M., and Yang, W. (2004) *Proc. Natl. Acad. Sci. U. S. A.* **101**, 2265–2269
47. Ling, H., Boudsocq, F., Woodgate, R., and Yang, W. (2004) *Mol. Cell* **13**, 751–762
48. Fiala, K. A., and Suo, Z. (2004) *Biochemistry* **43**, 2106–2115
49. Fiala, K. A., and Suo, Z. (2004) *Biochemistry* **43**, 2116–2125
50. Johnson, K. A. (1993) *Annu. Rev. Biochem.* **62**, 685–713
51. Johnson, K. A. (1992) in *The Enzymes* (Boyer, P. D., ed) Vol. 20, pp. 1–61, Academic Press, New York
52. Johnson, K. A. (1995) *Methods Enzymol.* **249**, 38–61
53. Pelletier, H., Sawaya, M. R., Wolfe, W., Wilson, S. H., and Kraut, J. (1996) *Biochemistry* **35**, 12762–12777
54. Pelletier, H., and Sawaya, M. R. (1996) *Biochemistry* **35**, 12778–12787
55. Abu Al-Soud, W., and Radstrom, P. (1998) *Appl. Environ. Microbiol.* **64**, 3748–3753
56. Rechkunova, N. I., Okhapkina, S. S., Anarbaev, R. O., Likhova, I. A., Degtyarev, S. K., and Lavrik, O. I. (2000) *Biochemistry (Mosc.)* **65**, 609–614
57. Miller, H., Prasad, R., Wilson, S. H., Johnson, F., and Grollman, A. P. (2000) *Biochemistry* **39**, 1029–1033
58. Shimizu, M., Gruz, P., Kamiya, H., Kim, S. R., Pisani, F. M., Masutani, C., Kanke, Y., Harashima, H., Hanaoka, F., and Nohmi, T. (2003) *EMBO Rep.* **4**, 269–273
59. Zinnen, S., Hsieh, J. C., and Modrich, P. (1994) *J. Biol. Chem.* **269**, 24195–24202
60. Woodsides, A. M., and Guengerich, F. P. (2002) *Biochemistry* **41**, 1039–1050
61. Choi, Y.-J., and Guengerich, F. P. (2004) *J. Biol. Chem.* **279**, 19217–19229
62. Zang, H., Harris, T. M., and Guengerich, F. P. (2005) *J. Biol. Chem.* **280**, 1165–1178
63. Johnson, R. E., Prakash, L., and Prakash, S. (2005) *Proc. Natl. Acad. Sci. U. S. A.* **102**, 12359–12364
64. DeLano, W. L. (2002) *The PyMOL User's Manual*, DeLano Scientific, San Carlos, CA